Microplasmas: Sources, Particle Kinetics, and Biomedical Applications

Felipe Iza, Gon Jun Kim, Seung Min Lee, Jae Koo Lee,* James L. Walsh, Yuantao T. Zhang, Michael G. Kong

Thanks to their portability and the non-equilibrium character of the discharges, microplasmas are finding application in many scientific disciplines. Although microplasma research has traditionally been application driven, microplasmas represent a new realm in plasma physics that still is not fully understood. This paper reviews existing microplasma sources and discusses charged particle kinetics in various microdischarges. The non-equilibrium character highlighted in this manuscript raises concerns about the accuracy of fluid models and should trigger further kinetic studies of high-pressure microdischarges. Finally, an outlook is presented on the biomedical application of microplasmas.

Introduction

The term *microplasma* is typically used to refer to discharges with dimensions that range from a few micrometers up to a few millimeters. Therefore, microplasmas are at least an order of magnitude smaller than the conventional low-temperature low-pressure discharges used for material processing in the semiconductor industry.[1] Microplasmas combine the potential of *low-temperature* plasmas with the advantages of being *micro*. The discharges create a highly reactive environment that contains charged particles, excited species, radicals, and photons, and the reduced dimensions enable low-power sources with small footprints suited for integration in microsystems and portable devices. Indeed, microplasmas represent a new realm in plasma physics that is receiving growing attention for its potential economic and technological impact in many scientific disciplines.[2]

Microplasmas can be dated back to the late 1950s[3] although it was not until the 1990s that research on microplasmas really started to take off. The renewed interest in the 1990s can be attributed to the extension of microfabrication techniques to build devices other than integrated circuits and the need for small plasma sources that could be integrated into newly envisioned microsystems. Since then, microplasma research has grown very rapidly, as evidenced by the increasing number of publications,[4–8] the organisation of an International Workshop on Microplasmas,[9] and the appearance of dedicated sections in major international plasma conferences. The continued research has broadened the application spectrum of microplasmas, which has included bio-medical applications,[10–15] displays,[16] radiation sources,[17–20] micro-chemical analysis systems,[21,22]

F. Iza, G. J. Kim, S. M. Lee, J. K. Lee
Department of Electronic and Electrical Engineering, Pohang University of Science and Technology, Pohang 790-784, Korea
E-mail: jkl@postech.ac.kr
F. Iza, J. L. Walsh, Y. T. Zhang, M. G. Kong
Department of Electronic and Electrical Engineering, Loughborough University, Leicestershire, LE11 3TU, UK

Plasma Process. Polym. **2008**, *5*, 322–344

DOI: 10.1002/ppap.200700162

Felipe Iza received a B.Sc. in engineering from the University of Navarra, San Sebastian, Spain, in 1997, and an M.Sc. and Ph.D. from Northeastern University, Boston, MA, in 2001 and 2004, respectively. From 1997 to 1999, he was with the Centro de Estudios e Investigaciones Tecnicas de Guipuzcoa (Ceit), San Sebastian, Spain. From 2004 to 2006 he was a postdoctoral fellow at Pohang University of Science and Technology (Postech), Pohang, South Korea, and joined that university as a Research Professor in 2006. Since 2007 he has been a Lecturer at Loughborough University, UK. His research interest is focused on experimental and computational low-temperature plasmas with special attention to microplasmas and atmospheric discharges for biomedical applications.

Dr. Iza is a Fulbright alumnus and a member of the Institute of Electrical and Electronics Engineers and the American Vacuum Society.

Gon Jun Kim received a B.Sc. in electronic and electrical engineering from Chung-Ang University, Seoul, Korea, in 2004 and is currently working towards a Ph.D. at Pohang University of Science and Technology (POSTECH). His research interests include computational low temperature plasmas and atmospheric-pressure glow discharges.

Seung Min Lee received a B.Sc. in electronic and electrical engineering from Kyungbook National University, Daegu, Korea, in 2004 and is currently working towards a Ph.D. at Pohang University of Science and Technology (POSTECH). His research interest is focused on computer simulations of plasma display panels, flat fluorescent lamps, and semiconductor processing.

Jae Koo Lee, an American Physics Society fellow, had his PhD from University of California, Berkeley in 1979 and his bachelor degree from Seoul National University in 1971. After working at General Atomics (fusion MHD theory) in San Diego, California for ten years, he became a tenured full Professor at Pohang University of Science and Technology in South Korea. He was the Chair of Korean Physics Society/Division of Plasma Physics for three years and is/was in the editorial boards of *J. Phys. D: Appl. Phys*. (current), *Plasma Sources Sci. Technol*. (2002-2005), and *Plasma Process. Polym*. (current). He has given a number of plenary or invited talks at international conferenes, e.g., the IEEE Conference on Plasma Science and others. He hosted as the LOC vice-chair the International Conference on Computational Physics (August 28–31, 2006, Gyeongjoo, South Korea) and served as a co-guest editor of a special issue in *Comput. Phys. Commun*. He has written five book chapters, and 100+ articles in international journals. Homepage at http://jkl.postech.ac.kr

James Walsh received an M.Eng. in systems engineering from Loughborough University UK, in 2004. He is currently working towards a Ph.D. degree in the area of ultra-short pulsed glow discharges within the plasma and pulsed power group (P^3G) at Loughborough University. His current research interests include the generation techniques of atmospheric pressure plasmas and their applications in the field of biomedicine.

Yuantao Zhang received a B.Sc. and M.Sc. in computational mathematics from Shandong University of Science and Technology and Dalian University of Technology, China, in 1999 and 2003, respectively, and a Ph.D. from Dalian University of Technology, where he majored in plasma physics in 2006. Now he is a postdoctoral researcher at Loughborough University, UK. His research interest involves the computational investigation on low-temperature plasmas, especially atmospheric pressure discharge plasmas.

Michael G. Kong received his B.Sc. and M.Sc. in electronics from Zhejiang University, P. R. China, and his Ph.D. in electrical engineering from the University of Liverpool, UK. After research and teaching posts at the Universities of Nottingham and Liverpool, he joined Loughborough University, UK, in 1999 where he now holds a Chair in Bioelectrical Engineering. He is a co-founder of a $5M Interdisciplinary Centre for Biological Engineering at Loughborough University. He was a Guest Editor for a special issue of IEEE Transactions on Plasma Science (Nonthermal Biomedical Applications of Ionizing Gases and Electromagnetic Fields, August 2006). His interests are non-thermal atmospheric discharges and electromagnetic fields as well as their applications to medicine and biology.

gas analyzers,[23,24] photodetectors,[25] microlasers,[26] dynamic millimetre and microwave devices,[27–29] microreactors,[30–34] propulsion systems,[35–37] aerodynamic flow control,[38,39] material processing,[40–44] and environmental applications.[14,45,46]

Microplasmas can be sustained in a wide pressure range. As expected from the Paschen law,[1] operation at high pressure favours the generation of small plasmas. Indeed, operation at atmospheric pressure is a natural choice for discharges with characteristic lengths of hundreds of microns. Nonetheless, operation at pressures as low as a few tens of mTorr[47] and as high as several tens of atmospheres[48,49] have also been reported. Operation at lower pressure is preferred for applications such as gas monitoring in the feed/exhaust pipes of a large-scale vacuum system.[50] For applications that require collisionless sheaths such as the sputter-coating of slender tubes, low-pressure operation is also preferred.[51,52] In general, however, microplasmas operate at higher pressure than conventional large-scale systems, and operation at atmospheric pressure is of particular interest for integration in microsystems and portable devices because this eliminates the need for vacuum pumps.

It is now well established that microplasmas, despite operating at high pressure, are non-thermal discharges. As a result, microplasmas share some fundamental physics with the low-pressure large-scale discharges used in the semiconductor industry. Microplasmas, however, have opened a new paradigm in plasma physics that still is not fully understood. While there is a strong application-driven interest in microplasmas, efforts should also concentrate on unravelling the underlying principles that govern microdischarges. Only through a deeper understanding can microplasmas be optimised for a given application.

The generation of microplasmas goes beyond scaling down large-scale reactors. In fact it is often true that microplasma sources have electrode arrangements that differ from those used in large-scale systems. Furthermore, even if a microplasma source is a miniaturisation of a large-scale device, its characteristics may differ. For example, the power efficiency of miniaturised planar-coil inductively coupled plasma sources depends strongly on the driving frequency, while a very weak dependence is observed in large-scale systems.[53]

Power consumption is an important factor that needs to be considered in the design of a microplasma. This is particularly important if the microplasma is to be integrated into a portable device. Although microplasmas can operate at very low power levels (<1W), the power densities achieved in these discharges ($kW \cdot cm^{-3}$ to $MW \cdot cm^{-3}$) are orders of magnitude larger than those in conventional large-scale systems ($W \cdot cm^{-3}$). Despite the high power density, departure from thermodynamic equilibrium is still possible thanks to the reduced dimensions of the discharges, large surface-to-volume ratios, and steep space gradients. In fact, one can argue that it is not possible to sustain a plasma in a large-scale system at the same power density as in a microplasma without the plasma becoming thermal and likely unstable.

To conclude this introduction, we should point out that the lifetime of a microplasma source is a factor that needs to be taken into account when judging the viability of this technology for a given application. While a lifetime of hours may be sufficient for single-use disposable devices, other applications may require devices with a much longer lifetime. The main factor that limits the lifetime of a microplasma source is typically the erosion of the electrodes by energetic particles. While some sputtering in large-scale systems may have a limited effect on the lifetime of the reactor, sputtering micrometer-sized electrodes can result in catastrophic failure of the microplasma source in just a matter of hours.[54,55] Electrode erosion not only limits the lifetime of the device but also is a source of undesired contamination. In general, electrodeless designs,[24] low gas temperatures, highly collisional sheaths,[56,57] protective layers (e.g., MgO layer in plasma display panels[58]), proper gas selection,[60] and low floating potentials (e.g., no bias and high-frequency excitation[60]) can improve the lifetime of the device.

The rest of this manuscript is organised as follows. In the next section, a review of the most typical microplasma sources is presented. Following a brief introduction to the diagnostics and computer simulations used for characterizing microdischarges, electron and ion kinetics in various microplasmas are then discussed. As an example of the many exciting applications of microplasmas, an outlook on biomedical applications is presented next. Finally, conclusions and future trends are discussed.

Microplasma Sources

Not all microplasma sources reported in the literature can be described in detail here. Nonetheless, most of the designs are presented, and the different strategies used to generate low-temperature microdischarges highlighted. To that purpose, microplasma sources are classified by the frequency of excitation and electrode configuration, following a typical classification for large-scale low-pressure plasmas. Although the criteria used are not unique and boundaries between some types of microplasmas are blurred, the classification groups devices that should be governed by similar underlying principles. The merits and limitations of different types of microplasmas are discussed, and an extensive reference list is provided for the interested reader. Before reviewing different microplasma sources, some general considerations are given.

DOI: 10.1002/ppap.200700162

General Considerations

Integrability and Portability

As suggested in the introduction, one should bear in mind that the success of microplasmas for a given application is subject not only to the miniaturisation of the plasma source but also to the integrability of the additional components needed for the generation of the plasma: power source and vacuum system. For this reason, atmospheric pressure plasmas are normally pursued as they eliminate the need for vacuum systems. Micropumps would increase the final cost of the system, are inefficient in achieving high vacuum levels, and may reduce the overall system reliability.

Regarding the power source, low-power operation is preferred, particularly for portable systems that run on batteries. Thus, low-temperature plasmas that operate close to room temperature are typically preferred as gas heating is normally not desired (although there are exceptions) and represents an energy loss.

Materials

Materials should have the right electrical properties, be easy to manipulate during fabrication, have an unlimited lifetime, and be inexpensive. However, such materials do not exist, so compromises must be made that depend on the application and the source design. Most microplasma sources have electrodes made of copper, gold, platinum, nickel, molybdenum, or tungsten. Copper is inexpensive but subject to oxidation. Thus, the performance of copper electrodes deteriorates with time if they are not encapsulated. Gold is preferred for its inertness and good electrical conductivity. Copper and gold, however, sputter easily, so they should not be exposed to energetic ion bombardment. Pt and Ni offer good corrosion resistance and have been used for direct current (DC) sources. Refractory metals such as Mo and W have also been used, typically for DC sources that operate at high temperatures. Applications where transparent electrodes are needed (e.g., plasma display panels) normally call for indium-tin oxide (ITO) electrodes. Because of the high resistivity of conductive oxides, these are normally used in conjunction with narrow metal electrodes in order to minimise electrical losses. Finally, doped silicon has also been used as an electrode material offering a straight integration with other semiconductor circuits.

Commonly used dielectrics are glass, mica, Kapton, and ceramics. Glass offers good chemical stability and easy integration with silicon devices. Mica and ceramics such as alumina and sapphire offer, besides chemical stability, a high dielectric constant and good thermal conductivity. Kapton and ceramic-reinforced Teflon laminates are inexpensive alternatives although they are subject to chemical etching if the plasma contains traces of nitrogen or oxygen (often the case in microplasmas operated at atmospheric pressure). DC and dielectric barrier discharges (DBDs) that rely on secondary electron emission often use films of materials with large secondary electron emission coefficients such as MgO.

Gases

The gas used to generate the plasma depends on the application. It is fair to say, however, that microplasmas operate mostly with noble gases (He, Ne, Ar, Xe). For operation at atmospheric pressure, He is typically preferred as it is easier to obtain diffuse glow-like discharges with He than with any other gas (the high thermal conductivity of He tends to prevent the onset of thermal instability). Besides offering a simpler chemistry, the use of noble gases also results in plasmas with lower gas temperature (better power coupling to the discharge), a critical aspect in some applications. Discharges that are open to the atmosphere, however, always involve mixing with air, and reactive species are present even if no reactive gas is fed to the microplasma directly. In order to control and achieve the desired reactivity, however, admixtures of molecular gases are often added to the noble gas. The amount of molecular gases that can be added is often limited to a few percent of the total gas flow because most microplasma sources are not capable of sustaining plasmas at higher concentrations. The reactive gas can be fed upstream (before the electrode region) or downstream (in the afterglow). Adding the reactive gases in the afterglow is in some cases technologically advantageous because it prevents contamination of the plasma source. In this case, metastables and excited species generated in the plasma active region transport energy downstream where the desired chemistry is prepared.

Finally it should be noted that the use of noble gases also affects the portability of the system (gas tank requirement). Furthermore, large flow rates (1–100 standard litres per min) are often used. For economical considerations, however, devices should operate with lower flow rates. Unfortunately, low-flow rate operation allows back-diffusion of atmospheric air into the plasma source and results in unstable operation or even extinction of the discharge. Indeed, operation in atmospheric air has proven quite elusive, and few plasma sources have succeeded in generating low-power atmospheric-pressure air plasmas.[60,61]

Frequency of Excitation (ω)

From a practical point of view, low-frequency operation (DC, alternating current (AC)) offers the advantage of requiring low-cost electronics. From a performance point of view, however, operation at high frequencies offers

some advantages: gas breakdown in high frequency fields requires lower voltages than in DC fields, and the potential across the sheaths decreases as $\approx\omega^{-2}$.[1] As a result, high frequency operation results in less energy being transferred to the ions (which in atmospheric pressure plasmas ends up mostly heating the background gas), more efficient plasma generation, and a longer device lifetime. Furthermore, although high-frequency power sources have traditionally been expensive, low-power high-frequency microplasmas can now make use of low-cost off-the-shelf amplifiers designed for mobile telecommunication applications.[63]

As in large-scale systems, pulsed operation of plasmas can be pursued for a variety of reasons. Pulsed operation can be employed to extract reactive negative ions that would otherwise remain trapped in the plasma. In addition, pulsed operation offers a means of reducing the average power consumption of the device, which can be critical in battery operated systems. But probably the main interest in pulsed operation is the possibility of generating discharges with high electron temperatures while the background gas remains close to room temperature. The high electron temperatures obtained during the turning on phases offer new chemistry equilibria not achievable with continuous wave excitation.[1,64]

Uniformity

Constricted discharges, patterns, and striations are often observed in microplasmas.[65–67] These phenomena are generally not completely understood and fundamental studies are still needed.[68] From a practical point of view, diffuse glow-like discharges are preferred since they are more controllable and provide a uniform treatment.

DC and Hollow Cathode Discharges

DC microplasmas are compact and easy to fabricate, and require simple electronics to drive them. As a result numerous groups have investigated these discharges. Different electrode configurations can be found in the literature: schematics of some designs are shown in Figure 1.

Gas breakdown in DC devices is described by the Paschen law, which states that the discharge breakdown voltage scales as a function of the product *pd*, where *p* is pressure and *d* the inter-electrode distance. For most gases, the minimum breakdown voltage is observed at *pd* values of 0.1–10 Torr · cm,[1] so operation at atmospheric pressure is typically pursued in gaps of ≈100 μm. Two factors, however, can lead to significant deviations from the Paschen curve. The first one is the onset of field emissions.[73] As the inter-electrode distance is reduced,

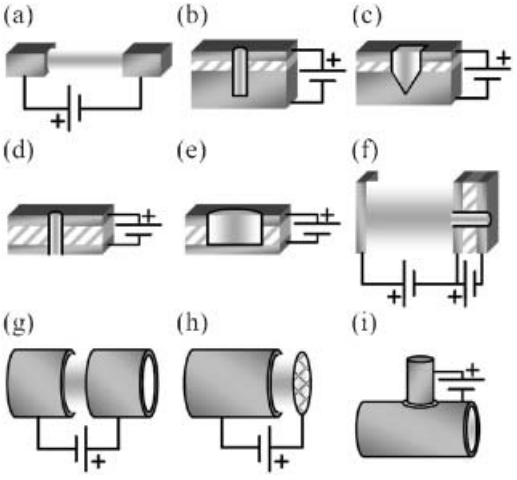

Figure 1. Schematic of various DC microplasma sources: a) parallel electrode,[54] b) cylindrical microhollow cathode,[69] c) inverted pyramidal microhollow cathode,[70] d) metal-insulator-metal microhollow cathode,[22] e) cathode boundary layer,[71] f) three-electrode source,[27] g) microtubes,[30] h) microtube with grid anode,[18] and i) microtube with inserted anode.[72] Solid colours represent metal electrodes and hatched objects represent dielectric materials.

the electric field in the gap increases and causes the onset of field emissions. Field emissions affect the left branch of the Paschen curve and are normally observed in DC discharges with gaps of less than ≈10 μm.[74,75] The threshold electric field for the onset of field emission depends on the electrode material, but for metals is typically on the order of $kV \cdot \mu m^{-1}$.[76] This threshold, however, depends strongly on the surface condition (contamination and roughness) of the electrode and can be further lowered by the presence of ions near the cathode (ion-enhanced field emissions).[77] Protrusions or nanostructures also enhance the local electric field and reduce the macroscopic emission threshold. For example, field emission from carbon nanotubes is normally triggered at 1–10 $V \cdot \mu m^{-1}$.[78] The other deviation from the Paschen curve takes place at very high pressures. As the pressure increases and the gas approaches the supercritical fluid state, statistical density fluctuations can result in the lowering of the breakdown voltage on the right branch of the Paschen curve.[48,49]

The main limitation of DC microplasmas is their short lifetime. Early DC microplasmas had lifetimes of hours.[54] Although operation at high pressure with low current densities and the use of low-sputtering yield materials extend the lifetime of DC microplasmas,[55,70] the limited lifetime remains an unresolved issue. The constant bombardment of the cathode by energetic particles not only results in the erosion of the electrode but also contaminates the discharge. This limitation, however, has been exploited to detect metals in liquids using micro-

DOI: 10.1002/ppap.200700162

fabricated liquid electrodes[79] and to generate metal vapor plasmas.[80] Although field emitters can be used to reduced the voltage required to sustain the discharge, experimental data in which nanotubes are deposited onto the cathode[81] and unpublished computational simulations carried out by the authors indicate that the field emitted current and the reduction in discharge voltage are too small. As a result, cathode erosion cannot be prevented and the initial performance enhancement achieved by the presence of field emitters is rapidly lost because of their deterioration by ion bombardment.

As in large-scale systems, hollow cathode configurations have also been used to achieve high-density microplasmas. When the cathode has a hollow geometry, secondary electrons emitted from the cathode are accelerated in the cathode sheath and sent towards the opposite side of the cathode where they are reflected back into the discharge.[1,3] In this way, high-energy electrons that otherwise would be quickly lost acquire a pendular motion. This pendular motion of the electrons increases the number of collisions that electrons undergo before they are lost to the anode, thereby significantly increasing the plasma density.[82] Hollow cathodes, however, also suffer from a limited lifetime because of the energetic ion bombardment. Furthermore, since the discharges can reach very high plasma densities (10^{14} to 10^{16} cm^{-3} at atmospheric pressure[83]), thermal damage to the electrode also needs to be considered. Gas temperatures of a several thousand degrees have been measured in hollow cathode microdevices.[84] For this reason, micro-hollow cathodes are normally fabricated with refractory and low sputtering yield materials such as Mo.

It should be noted that the pendular motion of electrons in a hollow cathode occurs only in a certain window of *pD* values (typically 1–10 Torr · cm). Here *p* is pressure and *D* the diameter (or characteristic length) of the hollow cathode. Experimental and computational studies show that the electron energy distribution function under these conditions has a high energy tail that extends to energies close to the applied voltage.[82,85,86] At larger *pD* values the pendular motion is lost because electrons do not reach the opposite side of the cathode with sufficient energy. Nonetheless, performance enhancement may still be observed thanks to the enhancement in ion and photon collection in the hollow geometry. As the size of the cathode is reduced, the Debye length can become comparable to the diameter of the cathode and the plasma may be pushed outside the hollow structure.[87]

DC microdischarges are typically operated in the abnormal glow mode, i.e., they display a positive differential impedance. This allows the parallelisation of microdischarges in arrays without the need for external ballast resistors.[18,88] In practice, however, current distribution across thin film electrodes affects the uniformity across the array and limits the number of microdischarges to <100.[88] Larger arrays of up to 250 000 microdischarges, however, have been demonstrated by using AC excitation with driving frequencies in the 1–20 kHz range.[88,89]

Finally, a three-electrode source using a microhollow cathode with an additional anode to extend a curtain of plasma has been reported by Schoenbach et al.[62] In that arrangement, the microhollow cathode behaves as an electron source, and the discharge in it acts as a virtual cathode for the DC discharge that extends from the microhollow cathode to the third electrode. Since electrons are not generated by ion impact, stable diffuse operation without the formation of arcs was demonstrated in air at atmospheric pressure.

Dielectric Barrier Discharges

Dielectric barrier discharges (DBDs) consist of two electrodes with at least one of them covered with a dielectric layer.[58,90] Numerous designs have been reported in the literature, with some shown in Figure 2. Since a dielectric layer prevents a DC current from flowing through the circuit, DBD discharges operate with AC excitation, typically in the kHz range.

The dielectric layers not only protect the electrodes, but also play a critical role in determining the characteristics of the discharge. Charge accumulation on the dielectric surfaces creates an electric potential that opposes the applied voltage and, as a result, limits the discharge current and prevents the glow-to-arc transition. At the same time, surface charge accumulated during one half period favours the discharge breakdown in the next half. This double role of the surface charges typically leads to the filamentation of the discharge, which is characterised by current spikes of much shorter duration than the AC excitation period. In some cases, filaments are stationary in space and create well-defined patterns,[66,94,95] whereas

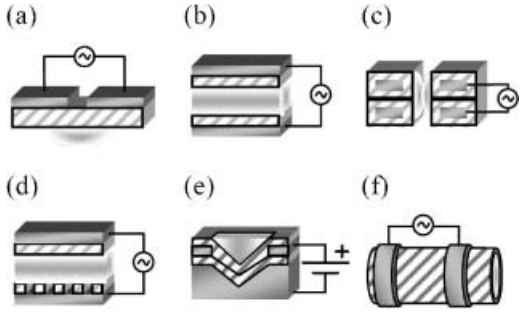

Figure 2. Schematics of dielectric barrier microdischarges: a) coplanar DBD,[16] b) parallel plate DBD,[91] c) coaxial DBD,[92] d) capillary plasma electrode discharge,[14] e) pyramidal DBD, [89] and f) capillary discharge/plasma pencil/plasma jet:[93] The solid colour represents metal electrodes and hatched objects represent dielectric materials.

in others, they are randomly distributed and the discharge appears uniform to the naked eye.[96,97] Besides the filamentary mode, diffuse (glow-like) discharges have also been observed.[97–100] For application purposes, diffuse discharges are preferred because they are more predictable and provide a more uniform treatment. However, diffuse DBDs tend to be low-density discharges. Seed electrons, photoemission, and photoionisation are known to play important roles in achieving a diffuse discharge.[101]

Operation of DBDs at frequencies other than the kHz range has also been pursued.[102–107] When operated at MHz frequencies, the dielectric layers act as a ballast impedance that allows the stable operation of the discharge. In this case, the current trace of the DBD does not present the sharp peaks representative of lower frequency DBDs and instead resembles the current trace of a capacitively coupled discharge.[103,104] For operation at low frequencies (tens of Hz) the dielectric layers have been replaced by high resistivity materials in what has become known as a resistive barrier discharge (RBD). The role of the resistive layer is that of a distributed ballast resistor that enhances the uniformity of the discharge.[107]

By far, the most popular application of micro-DBDs is the plasma display panel (PDP). Each pixel of a PDP consists of three DBD microdischarges (one for each primary colour).[16,58] They typically operate in Ne/Xe mixtures at ≈500 Torr (70 kPa). UV light generated by the de-excitation of Xe is converted into primary colours by the red, blue, or green phosphor covering the cell. PDPs are a clear example of how microdischarges can be paralleled to create large surface devices. PDPs larger than 100 inches and with more than two million pixels have already been commercialised.

A DBD discharge that has received significant attention is the microplasma jet (also referred to as 'plasma pencil' and 'capillary discharge'). A schematic is shown in Figure 2f.[64,93,108,109] In this device, gas flows through a dielectric tube and external ring metal electrodes are used to ignite the discharge. Although the device seems to sustain a uniform plasma plume, nanosecond resolved images have shown that the apparently uniform discharge is in fact a succession of 'plasma bullets'.[93] Intriguingly, the bullets travel at velocities that exceed the flow speed, initially accelerating as they travel downstream and travelling distances of up to several centimetres.[108] While there are lots of open questions regarding the underlying physics, the device has potential biomedical, material processing, and analytical applications.

Coronas

Corona discharges[58,90,110] consist of two asymmetric electrodes. One of the electrodes presents a sharply curved geometry whereas the other one may be flat. As a result, the electric field in between the two electrodes is non-uniform, with a much higher field strength around the highly curved electrode. When the electric field strength overcomes a threshold value, the corona discharge is originated around this electrode. Since the electric field is non-uniform, however, the discharge may be maintained around the highly curved electrode only. When brought in proximity to metal or dielectric objects, the discharge may extend to provide a plasma treatment to their surface. Corona, corona/DBD, and corona/glow modes have been discussed in the literature.[111–113] While most commonly used corona microplasmas employ pins (or needles), a slot configuration has also been explored.[114]

Corona discharges can be classified based on their polarity and frequency of excitation.[90] DC coronas are used in flow control applications,[38] whereas RF coronas have been suggested for biomedical applications[115,116] and material processing.[111,117] Despite the fact that corona discharges tend to be weak, the amount of radicals produced can be sufficient for some applications. Array configurations have also been explored to treat larger surfaces.[118]

RF Capacitively Coupled Plasmas

Capacitively coupled plasma (CCP) sources are widely used in the semiconductor industry and have been thoroughly studied over the last decades.[1] They typically operate at 1–100 MHz, so the electrodes can be protected with low sputtering yield materials even if these are insulating. Miniaturisation of these devices has been carried out by several groups:[119–122] schematics of some configurations are shown in Figure 3.

CCP microdischarges retain many similarities to large-scale low-pressure systems such as the capability to create glow discharges, and the α and γ operation modes.[128–130] High pressure discharges, however, tend to be constricted

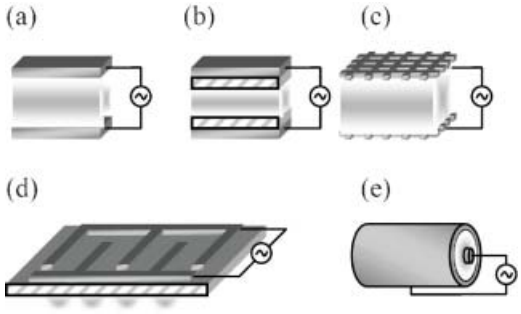

Figure 3. Schematics of RF capacitively coupled microplasmas: a) parallel plate with bare electrodes,[123] b) parallel plate with dielectric-covered electrodes,[124] c) grid electrodes,[125] d) comb electrodes,[126] and e) coaxial jet.[127]

DOI: 10.1002/ppap.200700162

and easily transit to arcs. For this reason, dielectric layers are often used as a means of stabilizing the discharge.[104]

CCP sources typically produce higher density plasmas than corona and DBD sources. However, since the electric field in a CCP is perpendicular to the electrodes, the ion density achievable with these devices is limited. As the power applied to the device increases, so does the energy lost by the ions accelerated in the sheath regions, which results in little plasma density gain.[1] Operation at higher frequencies can be pursued to reduce the voltage drop across the sheath, which makes the source more efficient in delivering the power to the electrons in the plasma. Reduction in the breakdown voltage in CCP sources[131] and higher efficiency in Monte Carlo simulations[132] have been reported when the frequency of operation is increased above the traditional 13.56 MHz. It is noted, however, that the improved energy transfer to the electrons as frequency is increased does not always result in an increase in plasma density. In some instances, the higher efficiency may translate to an increase in electron temperature.[133]

RF Inductively Coupled Plasmas

Inductively coupled plasma (ICP) sources are known for their high efficiency, relative simplicity, and controllability of the ion flux (density and energy).[1] Some schematics of miniaturised ICP (mICP) sources are shown in Figure 4.

mICP sources have no electrodes, and the induced electric field is parallel to the walls, thereby minimizing energy losses in the sheath as well as erosion and contamination. As a result, mICPs can be operated for years without signs of deterioration. Unfortunately, ion densities as large as in large-scale systems have proved difficult to obtain with small-size mICP sources.[137–139] The fact that the inductance of the coil decreases faster than the parasitic resistance, as well as a higher surface-to-volume ratio as the dimensions are reduced, limit the performance of mICPs. Nonetheless, plasma densities of $\approx 10^{11}$ cm^{-3} in argon at 350 mTorr (46.7 Pa) have been reported using a 5 mm planar coil while consuming 1 W.[137]

Opposite to what is commonly true in large systems, the performance of mICP sources depends on the operation frequency.[137] It has been observed that the power efficiency improves when the frequency of operation increases, so mICPs typically operate in the VHF and UHF bands (hundreds of MHz).[135–139] High frequency operation also favours the ignition of the discharge as the RF frequency can be brought closer to the electron-neutral collision frequency.[138] The performance improvement obtained by increasing the driving frequency, however, is only possible while the frequency is small compared to the self-resonance frequency of the coil[138] as well as to the electron collision frequency.[137] An increase in the coil AC resistance may also limit the maximum frequency of operation.[137]

mICP sources operate best at relatively low pressure (0.1–10 Torr, 0.01–1 kPa).[140] At atmospheric pressure, the current needed in the coil to sustain a pure inductively coupled plasma is too large. Nonetheless, mICPs aided by thermionic emission from a filament[135] and capacitive coupling across legs of a serpentine[136] have been used to sustain hybrid discharges at atmospheric pressure.

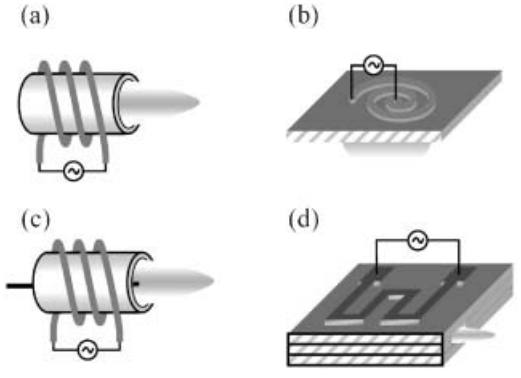

Figure 4. Schematics of inductively coupled microplasma sources: a) coil,[134] b) planar spiral,[134] c) coil + filament,[135] and d) serpentine.[136]

Microwave Plasmas

Large microwave plasma sources (e.g., helicon, electron cyclotron resonance, and surface wave discharges) are known for their high efficiency.[1] The dimensions of these devices, however, are strongly related to the wavelength of the excitation field. Therefore, scaling down these devices is problematic. A microwave plasma source a few millimetres in size would require frequencies of operation of 10 to 100 GHz, which is currently impractical. Several microplasma sources operating in the GHz range, however, have been reported.[61,63,141–150] These devices use microwave guides (microstrips, coaxial guides, and striplines) instead of lumped element circuits to deliver power to the plasma. In most designs, the plasma dimensions are much smaller than the excitation wavelength and the discharges can be regarded simply as capacitively coupled plasmas operated at GHz. Microstrip and stripline technologies, however, have also been used to generate plasmas with dimensions comparable to the RF excitation wavelength.[151] Schematics of microwave microplasma sources are shown in Figure 5.

Microwave plasma sources based on microstrip structures are of particular interest for their simplicity and

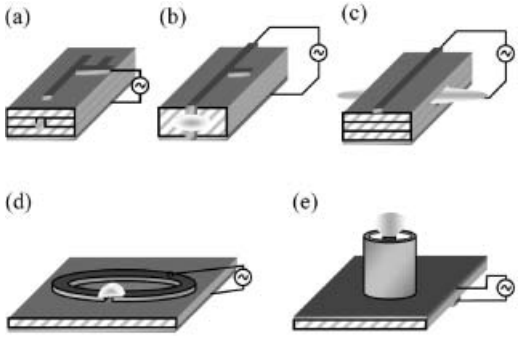

Figure 5. Schematics of microwave microplasma sources: a) microstrip linear resonator,[141–143] b) microstrip linear resonator with engineered end,[144] c) surface wave launcher based on microstrip technology,[144] d) $\lambda/2$ microstrip split-ring resonator,[61,63,144,145] and e) coaxial source. [51,52,149,150]

robustness. Radiation losses and interference are minimised by the use of waveguides, so the sources are more efficient and less prone to perturbations than other microplasma sources operated at UHF or with nanosecond pulses. Although some microwave microplasmas can be regarded as capacitively coupled sources, the use of a high-frequency excitation significantly enhances the performance of the device with respect to RF CCPs. Since the sheath potential scales as $V_s \approx \omega_{rf}^{-2}$,[1] the energy transferred to the ions in the sheath is reduced, so microwave excited microplasmas are more efficient and have longer lifetimes.

Although power sources in the GHz range have traditionally been expensive, preventing the integration of microwave microplasmas into low-cost portable systems, this is no longer the case. Power sources developed for mobile telecommunication applications are now readily available, opening the possibility of low-cost low-power microplasma sources.[63]

Diagnostics and Simulations of Microplasmas

The reduced dimensions of microplasmas make experimental characterisation of the discharges very challenging. The probe diagnostics commonly used to characterise large-scale plasmas unavoidably perturb microplasmas, and the interpretation of the measured current/voltage curves is further compromised by the lack of appropriate collisional probe theories.

Due to these limitations, optical diagnostics are typically preferred. These are non-invasive although their interpretation is not always easy. Furthermore, space- and time-resolved measurements require complex experimental setups,[152,153] and, occasionally, scaled-up versions of microplasmas have been used to characterise the discharges.[154]

Given its relative simplicity, optical emission spectroscopy is the most commonly used optical diagnostic technique. The intensity ratio of emission lines has been used to estimate the electron temperature,[144] Stark splitting and broadening to determine the electron density and electric field,[153] and the rotational temperature of molecular traces to estimate the neutral gas temperature.[154,155] Absorption spectroscopy has also been used to estimate the neutral gas temperature from the Doppler profile of absorption lines.[109]

Laser-aided diagnostics are more complex than emission/absorption spectroscopy, but have been gaining attention in recent years. Although laser-aided techniques have been used successfully in the study of low-pressure large-scale systems, collisional quenching and scattered radiation from surfaces make laser-aided diagnostics quite challenging for the study of high-pressure microplasmas. Nonetheless, Thomson scattering has been used to determine the electron density,[156] laser absorption to determine metastable concentrations,[152] laser-induced fluorescence (LIF) to determine surface charges in a DBD discharge,[157] and two-photon LIF spectroscopy to measure absolute concentrations of radicals.[158]

Finally, mass spectrometry can also contribute to the study of microplasmas. Microplasmas have been used as ion sources for mass spectrometry,[109] and molecular beam mass spectrometry has been used to determine radical and neutral densities in a discharge generated by a plasma needle.[159] Ion mobility[160] and differential ion mobility[161] spectrometry are well suited for characterizing microplasmas because of the highly collisional regimes typically encountered in microdischarges.

Given the experimental challenges, computer simulations provide a valuable alternative for studying microdischarges. Fluid (or hydrodynamic), particle-in-cell, and hybrid methods are commonly used to simulate low-temperature plasmas.[162,163] Fluid simulations solve a set of moments of the Boltzmann equation and are capable of handling multiple species, a large number of reactions, and hydrodynamic effects, all in a relatively short simulation time. Built-in in the fluid model, however, is the assumption that the electron energy distribution function can be inferred from local values of the electric field. This limitation prevents fluid codes from capturing non-local electron kinetics. Despite operating at high pressure, non-local kinetics can take place in microdischarges because of the large electric fields and the reduced dimensions of the discharge. For example, the electron energy probability function of a micro hollow cathode discharge has a very pronounced high energy tail that is not in equilibrium with the local electric field. Striations in PDP cells is another example of non-local electron kinetics

DOI: 10.1002/ppap.200700162

in a dielectric barrier microdischarge.[164] As it is discussed later, low-energy electrons in RF CCP microdischarges are also found not to be in local-equilibrium with the electric field.[165]

Particle-in-cell simulations overcome this limitation of fluid models. However, they are computationally very expensive. As a result, a reduced number of species, simplified chemistry, and no hydrodynamic effects are typically considered in particle simulations. Furthermore, particle simulations need to resolve the collision frequency of all the particles, so very small time steps are required to simulate high-pressure discharges. Slow particle diffusion and small time steps can turn particle simulations of high-pressure discharges into a daunting task.

In an attempt to overcome the limitations of fluid and particle codes, hybrid codes are designed to take the strengths of both approaches while circumventing their limitations. This simulation technique make it possible to study microdischarges by integrating multiple physics within one simulation.[87]

Limited computational work has been published regarding microplasmas. The number of studies, however, is growing, and they are contributing to the advancement of the field.[56,82,87,112,113,165–168] Although the fundamentals of the computational models remain the same, computer modeling of high-pressure microdischarges is in practice more challenging than the modeling of low-pressure discharges. Because of the high collisionality encountered in microplasmas, smaller time steps, more significant species (e.g., dimers), additional collision processes (e.g., step ionisation and three body collisions), and hydrodynamic and thermal effects, etc. need to be considered. Furthermore, despite the high collisionality, the non-equilibrium character of microplasmas also requires the study of kinetic effects not captured by pure hydrodynamic models.

Electron and Ion Kinetics

In order to optimise microplasmas for a particular application, a fundamental understanding of the physics governing the discharges is required. Unfortunately, limited fundamental studies have been reported to date. This is in part a result of the strong application-driven interest in microdischarges but also because of the difficulty in obtaining accurate diagnostics. One important piece of information required to pinpoint the underlying physics in non-equilibrium discharges is particle kinetics. Scarce data have been published regarding particle kinetics in low-temperature microplasmas as most studies found in the literature are based on fluid models, which provide no kinetic information.

In this section, we discuss electron and ion kinetics in various microplasmas based on recent computer simulation results. The kinetic information that is presented was obtained using 1- and 2-dimensional (1d3v and 2d3v) particle-in-cell Monte Carlo collision simulations (PIC-MCC). Open source codes (XOOPIC[169] and XPDP1[170]) and codes developed by the authors (APPS2[51,82]) were used in the study. The high computational cost of PIC-MCC simulations limited the number of species and reactions that could be accounted for in the simulations. The present studies included electrons and singly charged ions (Ar^+, He^+, Ne^+, and Xe^+) in the models. In all the simulations the gas temperature was assumed to remain close to room temperature (a reasonable approximation for many microplasmas although this assumption needs to be revisited for some others), so the background neutrals were uniformly distributed in space ignoring any thermal gradient.

Elastic, excitation, and ionisation electron–neutral collisions were accounted for in the simulations. Coulomb collisions were not included owing to computational constraints. Coulomb collisions tend to maxwellianise the electron distribution function and their influence should be the subject of future studies of high-density microdischarges. In particular, electron/electron collisions should be included when the energy transfer in electron/electron collisions becomes comparable to that in electron/neutral collisions, i.e. $0.5\nu_{e\text{-}e} \approx \delta\nu_{e\text{-}n}$. Here $\nu_{e\text{-}n}$ is the electron/neutral collision frequency (≈THz at atmospheric pressure), $\nu_{e\text{-}e}$ the electron/electron collision frequency and $\delta \approx 2\ m_e/M \approx 10^{-4}$. Therefore, Coulomb collisions should be considered in microdischarges with densities above $\approx 10^{14}$ cm^{-3}. For ions, elastic scattering and charge exchange collisions were included in the models.

A detailed description of the secondary electron emission processes in atmospheric-pressure discharges should incorporate contributions from ions, metastables, hot neutrals, and photons. Furthermore, as the discharge gap shrinks, field emission also needs to be taken into account.[74,75] However, for simplicity, an effective ion-induced secondary electron emission coefficient (γ) was used in the simulations. Constant ion-induced secondary electron emission coefficients $\gamma_{Ar+} = \gamma_{He+} = 0.1$ were used for the Ar and He discharges, whereas a secondary electron emission coefficient that accounts for the energy and angle of the incident ions was used for the Xe/Ne discharges.[171]

Low-Pressure Large-Scale Plasmas versus High-Pressure Microdischarges

Both low-pressure large-scale plasmas and high-pressure microplasmas generate non-equilibrium low-temperature

discharges. Their size and operation pressure, however, differ by orders of magnitude. Therefore, it is of interest to make some general remarks regarding the similarities and differences between them. To that end, Figure 6 compares various plasma parameters in a conventional low-pressure large-scale Ar discharge with those in a He atmospheric-pressure microplasma.

At atmospheric pressure, the electron/neutral collision frequency (ν) is much larger than the RF (ω_{rf}) driving frequency (Figure 6a,b), so the bulk plasma is mainly resistive, i.e., the inductive behaviour due to the electron inertia often encountered in low-pressure discharges can be ignored ($\nu \gg \omega_{rf} \Rightarrow \sigma \approx \sigma_{DC}$). Under these conditions bounce resonance motion[172] is also inhibited by frequent collisions. Furthermore, while the electron thermal velocity (v_{th}) is comparable in the two, the product collision frequency times discharge size (νL) is typically ≈100 times larger in a microplasma. As a result, the condition $\nu L/v_{th} \gg 1$ is normally satisfied in microplasmas, so collisionless heating[1] is negligible. In other words, ohmic (collisional) heating is the dominant heating mechanism in microdischarges. As a result of the high collisionality, electric fields larger than those required to sustain a discharge at low-pressure are required to sustain a high-pressure microdischarge.

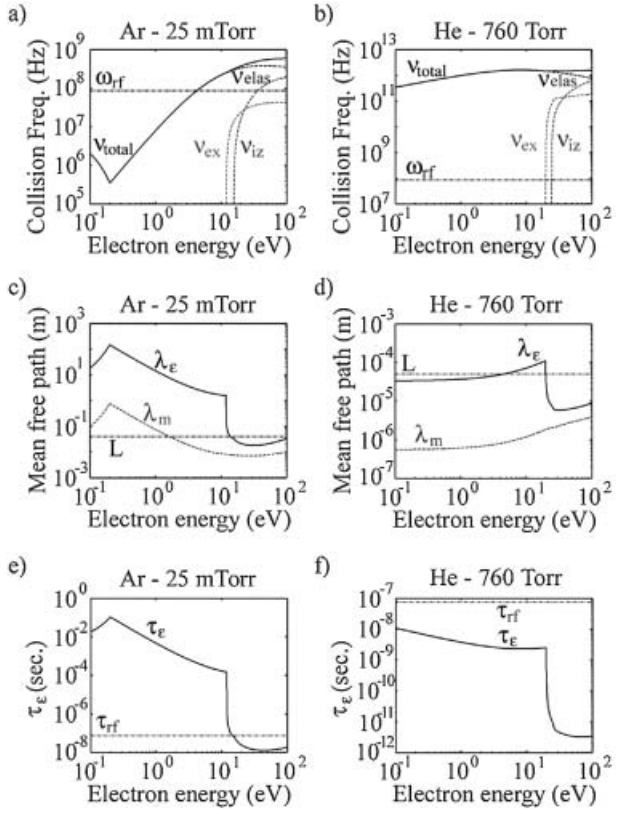

Figure 6. Comparison between a low-pressure Ar RF (13.56 MHz) discharge (a,c,e) and an atmospheric-pressure He RF (13.56 MHz) microplasma (b,d,f). a,b) Comparison between the electron/neutral collision frequencies (ν_{total}, ν_{elas}, ν_{ex}, and ν_{iz}) and the RF driving frequency (ω_{rf}). c,d) Comparison between the electron mean free path (λ_m), the electron energy relaxation length (λ_ε), and the characteristic length of the system (L). e,f) Comparison between the electron energy relaxation time (τ_ε) and the RF period (τ_{rf}).

It is normally accepted that non-local electron kinetics are important in describing low-pressure discharges (<100 mTorr, 13 Pa), while local kinetics (and fluid models) become valid at higher pressure. It would be erroneous, however, to assume that in a microdischarge the electrons are in local equilibrium with the electric field simply because the discharge operates at atmospheric pressure. In fact, the large electric fields and the reduced dimensions encountered in microdischarges contribute to a departure from the local kinetics regime.

The transition from the local to the non-local regime takes place when the electron energy relaxation length becomes comparable to the length of the spatial inhomogeneity of the electric field. In low-pressure plasmas, this length is approximately the size of the discharge gap, and electrons are found in the local or the non-local regime depending on the discharge conditions. For the 25 mTorr (3.3 Pa) Ar discharge used as an example in Figure 6c, low-energy electrons are in the non-local regime ($\lambda_\varepsilon > L$) whereas high-energy electrons are marginally in the local regime ($\lambda_\varepsilon < L$). The distinction between low- and high-energy electrons is made because of the much faster collisional energy loss of electrons with energy above the inelastic (excitation) threshold. If the system length (L) in Figure 6c had been 1 cm instead of 4 cm, all the electrons would be in the non-local regime. Several effects such as negative power absorption, non-monotonous electric field profiles, anomalous skins, and striations are related to non-local electron kinetics.[173–176]

Similarly, low-energy electrons in an atmospheric-pressure microdischarge (Figure 6d) may not be in local equilibrium with the electric field ($\lambda_\varepsilon > L$). Indeed, non-local effects such as striations have been observed in high-pressure microdischarges and linked to the non-locality of

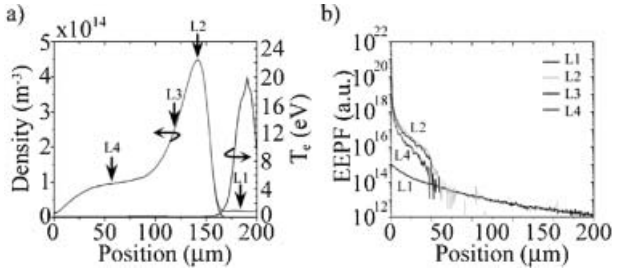

Figure 7. He DC microdischarge at atmospheric pressure.[177] a) Density and effective electron temperature profiles. b) EEPF at the four locations marked in (a). (Reprinted with permission, © 2007 IEEE.)

DOI: 10.1002/ppap.200700162

low-energy electrons.[65,164] The energy relaxation length (λ_ε) of electrons in the elastic energy range ($\varepsilon < 20$ eV for He) is ≈50 μm (Figure 7d), which is of the same order as the width of the potential well experienced by low-energy electrons in a 100 μm discharge. It should be noted that, in microdischarges, the sheaths typically occupy a much larger fraction of the discharge gap than in low-pressure discharges,[165,166] so the width of the potential well experienced by the electrons is significantly shorter than the gap size.

Unlike in low-pressure discharges, the electron energy relaxation time in an atmospheric microdischarge ($\tau_\varepsilon \approx 5$ ps to 10 ns) is shorter than the RF period ($\tau_{13.56\ \mathrm{MHz}} \approx 74$ ns) (Figure 6e,f). As a result, the electron energy distribution function is strongly modulated by the driving frequency, especially in the inelastic energy range. Because of this fast energy relaxation time, even RF capacitively coupled discharges at atmospheric pressure can be seen as a succession of DC discharges sustained at different voltages.

Electron Energy Probability Function (EEPF)

Electrons play a key role in sustaining the plasma as well as in establishing the chemical reactivity of the discharge. For this reason, determining the electron energy probability function (EEPF) and understanding its formation is of paramount significance. This section presents the EEPF in various microplasmas and shows that the EEPF, even in atmospheric-pressure microplasmas, is far from thermodynamic equilibrium. This implies that results obtained with fluid models that assume a Maxwellian EEPF should be interpreted cautiously. It is also noted, however, that current PIC models account only for a subset of the reactions normally considered in fluid models and, therefore, further studies are still needed for a quantitative comparison between hydrodynamic and kinetic results.

EEPF in DC Microplasmas

Figure 7 shows the density profile, the effective electron temperature, and the EEPF in a DC microdischarge. The atmospheric-pressure He plasma was generated between two parallel electrodes using a current source (1 A · cm^{-2}). The gap size between the two parallel plate electrodes was 200 μm. No fundamental differences have been observed between the EEPF in the DC microdischarge and conventional large-scale low-pressure DC discharges operated at the same *pd* value.[177]

The EEPF in the bulk plasma (negative glow) is typically bi-Maxwellian. It comprises a large number of low-energy electrons that are confined by the ambipolar potential, and mid-energy electrons capable of escaping the discharge. The latter carry the current to the anode and have a higher temperature than the low-energy electrons.[177] In addition to low- and mid-energy electrons, high-energy electrons are generated in the cathode sheath as a result of the acceleration of secondary electrons. These electrons can reach energies close to the applied voltage and are not in equilibrium with the local electric field. Depending on the *pd* value, the energetic electrons penetrate deep into the bulk plasma or relax their energy near the sheath-bulk boundary. For the conditions of the example in Figure 7, *pd* is ≈15 Torr · cm and electrons barely penetrate into the bulk ($L \approx 200\ \mu\mathrm{m} \gg \lambda_\varepsilon \approx 1\ \mu\mathrm{m}$). As shown in Figure 7, the electron temperature in the cathode sheath (approx. inversely proportional to the slope of the EEPF) is very high (≈20 eV) but rapidly decreases as electrons reach the bulk plasma where the electric field is much smaller and high-energy electrons rapidly lose their energy through inelastic collisions.

Thus, three electron groups can be identified in the discharge: low energy electrons trapped in the bulk plasma, mid-energy electrons that escape to the anode, and high energy electrons that are created in the cathode sheath. The transition between low-and mid-energy electrons occurs at the energy that corresponds to the confining potential on the anode side (≈2 eV in the example) and the transition between mid- and high-energy electrons to the threshold energy for inelastic collisions (≈20 eV for He). These three electron groups can also be identified in other microdischarges.

EEPF in Microhollow Cathodes

When the *pd* value decreases, high energy electrons penetrate deeper into the bulk plasma and eventually start reaching the anode with significant energy. High-energy electrons that reach the anode represent an

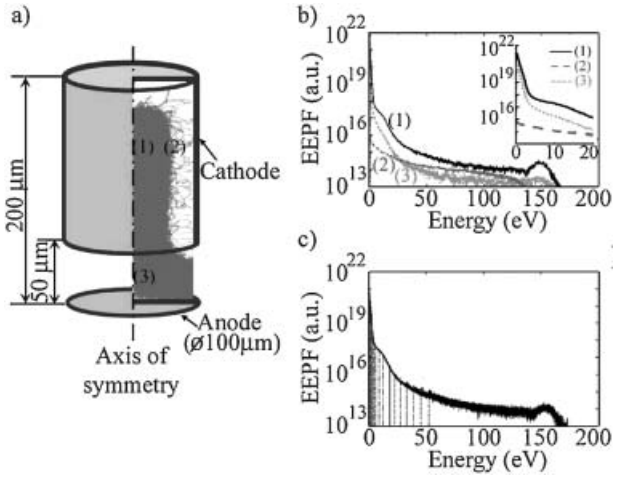

Figure 8. Microhollow cathode discharge in Ar at 10 Torr (1.3 kPa). a) Trajectories of electrons showing the pendular motion of the electrons.[82] b) EEPF vs. kinetic energy at various locations showing the high energy tail created by pendular electrons.[82] c) EEPF vs. total energy at various locations.

undesired loss because the energy invested in accelerating the electrons in the cathode sheath is directly transferred to the anode instead of being invested in ionisation/excitation. To prevent the loss of high-energy electrons, a cathode with hollow geometry can be employed. The hollow geometry causes high-energy electrons to oscillate inside the cathode, which prevents their premature loss. This longer confinement increases their chances of undergoing ionizing collisions, so a more efficient discharge can be generated (Figure 8a).[82] This retention of high energy electrons is evidenced in the EEPF of hollow cathode discharges as a high energy tail that extends virtually to the applied voltage.[82,85,86] Figure 8b shows the EEPF in a microhollow cathode discharge operated in Ar at 10 Torr (1.3 kPa). The *pD* value in this case is 0.1 and electrons accelerated in the cathode sheath cross the bulk plasma to reach the sheath at the opposite side of the cathode where they are reflected back into the discharge (Figure 8a). Here *p* is pressure and *D* the cathode diameter.

The fact that electrons are in non-local equilibrium with the electric field can be explicitly shown by plotting the EEPF as a function of the total (kinetic + potential) energy. This is done in Figure 8c, where the overlap of the EEPFs at various locations within the cathode indicates that electron kinetics are non-local.[173] Thus, in hollow cathode discharges with pendular electrons, the three electron groups observed in the DC discharge are also present. However, the high-energy tail present at the centre of the hollow cathode discharge (Figure 8b) disappears near the cathode sheath edge in parallel plate discharges operated at higher *pd* values (Figure 7b). A more subtle difference between the parallel plate and the hollow cathode discharge considered in the examples is the threshold energy between low- and mid-energy electrons. The presence of a large flux of energetic electrons to the anode in the hollow cathode discharge requires a higher confining potential[178,179] than in the parallel plate case, so the transition between low- and mid-energy electrons takes place at ≈4 V instead of ≈2 V.

EEPF in RF CCPs

The time resolved EEPFs in 200, 100, and 75 μm He RF discharges operated at atmospheric pressure are presented in Figure 9.[165,180] The discharges are driven by a current source at 1 A · cm^{-2} and 13.56 MHz. The EEPF in the centre of the discharge, the space-averaged EEPF, and the space- and time-averaged EEPF are shown in the figure. As already discussed, the EEPF is strongly time modulated because of the fast electron energy relaxation ($\tau_\varepsilon < \tau_{rf}$).

The three electron groups observed in the DC microdischarges can also be identified in these RF microdischarges (Figure 9a–c). In the centre of the discharge (Figure 9d–f), the high energy tail is observable only when the width of the sheaths is comparable to half the gap size (100 and 75 μm discharges, Figure 9e,f). For discharges sustained in larger gaps, high-energy electrons lose their energy before reaching the discharge centre (200 μm discharge, Figure 9d). Therefore, the presence of high-energy electrons in the centre of the discharge of a high-pressure RF microdischarge is related to the sheath width. This contrasts with the typical situation encountered in low-pressure discharges where the presence of high-energy electrons in the centre of the discharge is related to the non-locality of high energy electrons.[181]

The time- and space-averaged EEDFs in the three microdischarges are shown in Figure 9g–i. The temperature of the high-energy electrons (which is determined by

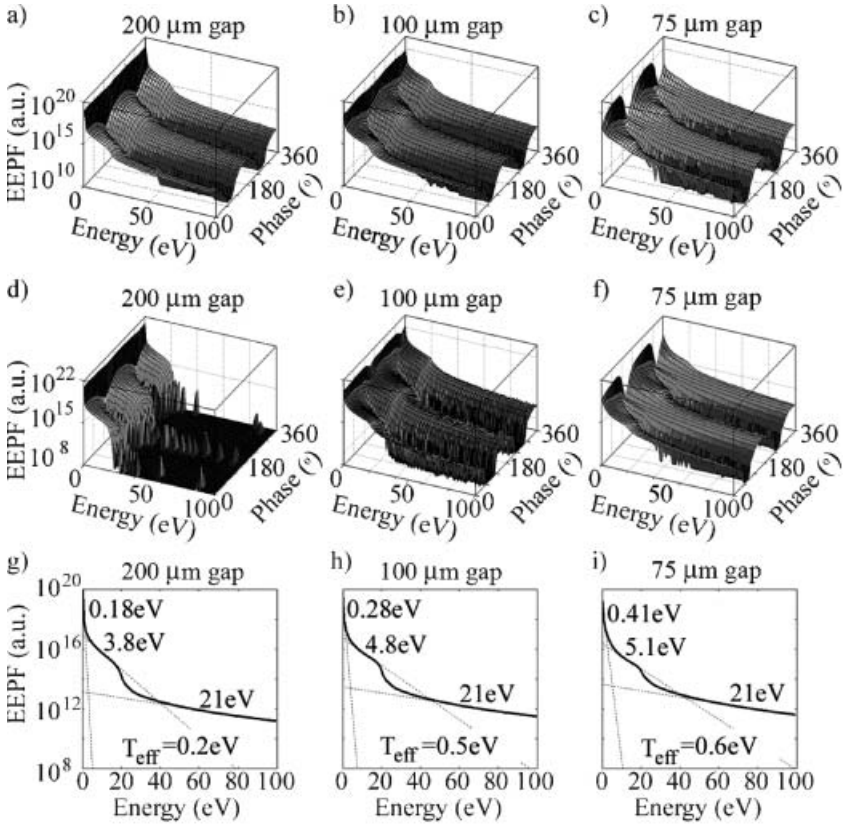

Figure 9. Time evolution of the EEPF in three atmospheric-pressure He microplasmas driven at 1 A · cm^{-2}. a–c) Space-averaged EEPF. d–f) EEPF in the centre of the discharge. g–i) Space- and time-averaged EEPF. Figure reprinted with permission from ref.[165]. Copyright 2007 American Physical Society.

DOI: 10.1002/ppap.200700162

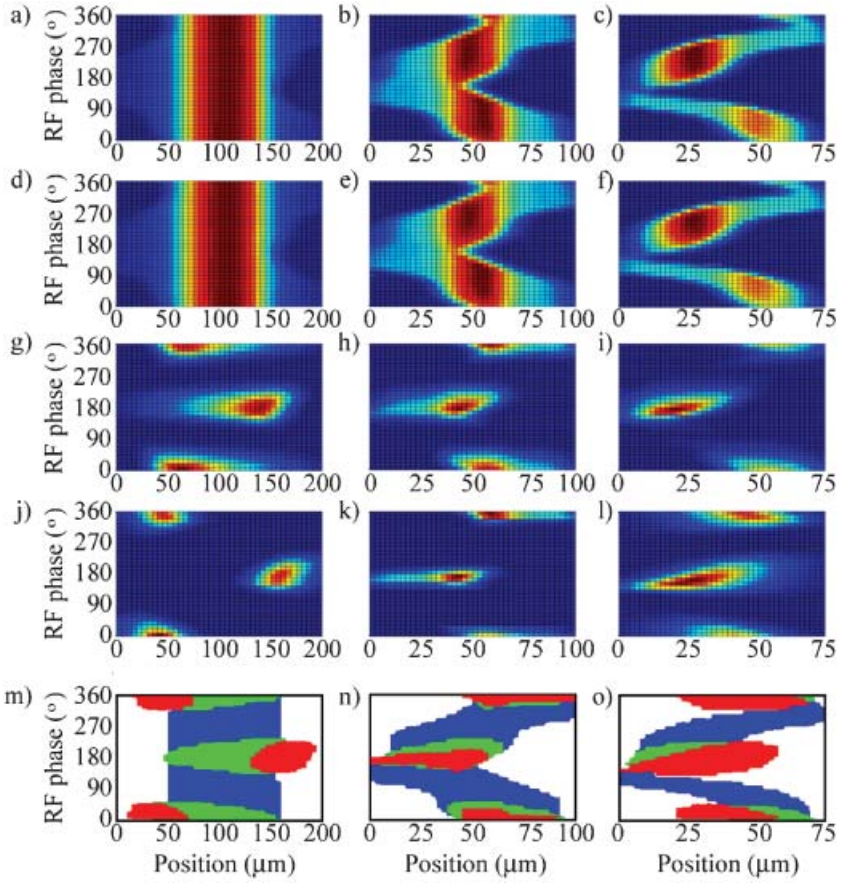

Figure 10. Time evolution of the normalised electron density in RF atmospheric-pressure He microplasmas sustained in gaps of 200 (a,d,g,j,m), 100 (b,e,h,k,n), and 75 μm (c,f,i,l,o).[165,180] a–c) Total electron density. d–f) Normalised density of electrons with energy $\varepsilon < 4$ eV. g–i) Normalised density of electrons with energy $4\ \text{eV} < \varepsilon < 20$ eV. j–l) Normalised density of electrons with energy $\varepsilon > 20$ eV. m–o) Superposition of the spatio-temporal density profiles of the three electron groups. Figure reprinted with permission from ref.[165]. Copyright 2007 American Physical Society.

the electric field in the sheaths) is the same for the three microdischarges. This is because the sheath remains virtually unaffected by the change in gap size. As shown in Figure 10, the reduction in gap size is accommodated by the reduction of the bulk plasma region, and the electric field in the sheath region remains unaltered (not shown explicitly). The temperature of low- and mid-energy electrons (and therefore the effective temperature), however, increases as the gap size is reduced. This is a result of the higher electric field experienced by the electrons in the bulk plasma. The increase of the electric field is related to the incomplete shielding of the applied potential by the sheaths. In very small gaps (Figure 10c), the bulk plasma oscillates between the electrodes, and time-averaged quasi-neutrality is lost.[165,180]

Figure 10j–l indicates that high-energy electrons are generated only in the sheaths and mostly when they are fully expanded. This situation is consistent with the γ mode of capacitively coupled plasmas. While low pressure RF plasmas can operate in the α and γ modes and experimental and simulation studies have demonstrated the existence of both modes in millimetre size atmospheric pressure micro-discharges,[128–130] no experimental data has confirmed the existence of both modes in smaller microdischarges. Indeed, for the geometries used in the three RF microdischarges, the discharges extinguish without transitioning to the α mode when the driving current is decreased.[165]

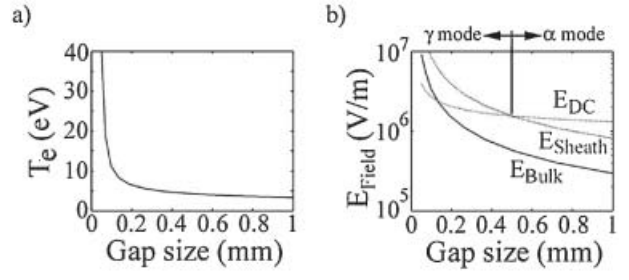

Figure 11. Global model of an atmospheric-pressure Helium plasma driven at 13.56 MHz with $n_e = 10^{11}$ cm^{-3}. a) Electron temperature and b) electric field in the bulk and in the sheath as a function of the gap size. E_{DC} in (b) is the DC breakdown electric field for helium at atmospheric pressure [1] assuming $\gamma = 0.1$.

The absence of the α mode is qualitatively justified by the following argument. Figure 11 shows the electron temperature and bulk electric field in an RF atmospheric-pressure helium discharge as a function of the discharge gap size as calculated using a global model:[1] the particle balance equation (1) is used to determine the electron temperature, and the local energy balance (2) to obtain the electric field required to heat the electrons.

$$n_g K_{iz} = \mu_i \frac{kT_e}{e} \left(\frac{\pi}{L}\right)^2 \tag{1}$$

$$\mu_e e E^2 = n_g \left(3 \frac{m_e}{M_{He}} kT_e K_{el} + \varepsilon_{ex} K_{ex} + \varepsilon_{iz} K_{iz}\right) \tag{2}$$

Here n_g is the background neutral number density; K_{el}, K_{ex}, and K_{iz} are the elastic, excitation, and ionisation rate constants; μ_e and μ_i are the electron and ion mobility; e is

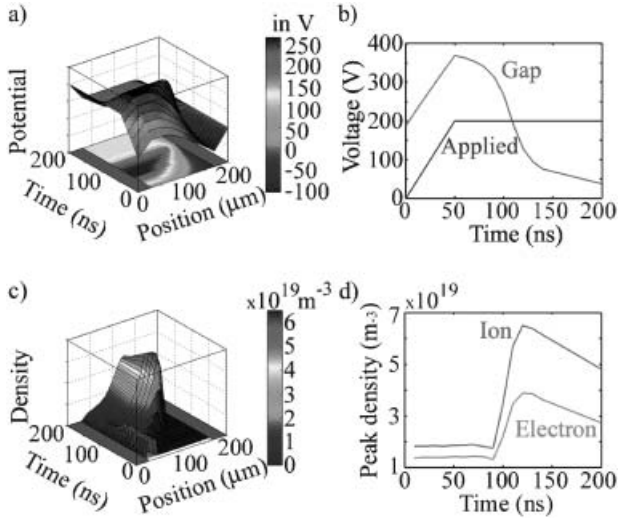

Figure 12. Potential and density profiles in a Ne/Xe(5%) DBD microdischarge at 300 Torr (40 kPa). a) Time evolution of the potential profile. b) Applied voltage and gap voltage as a function of time. c) Time evolution of the electron density profile. d) Maximum electron and ion densities as a function of time. The discharge is operated at 200 V/150 kHz and the results presented account for residual charges on the dielectrics from previous pulses.

the elementary charge; m_e and M_{He} are the electron and helium atom mass; and k is the Boltzmann constant.

It is further assumed that the current in the sheaths is dominated by the displacement current, and that the bulk conductivity approaches the DC limit (reasonable assumptions for an atmospheric pressure discharge). With these assumptions, current continuity requires the electric field in the sheaths to be larger than the field in the bulk plasma by a factor of $\approx \omega_{pe}^2/(\omega_{rf}\,\nu)$. Here ω_{pe} is the electron plasma frequency, ω_{rf} is the RF driving frequency, and ν is the electron/neutral collision frequency.

As the gap size (L) is reduced, the surface-to-volume ratio and the particle losses to the wall increase. As a result, the electron temperature and the electric field needed to sustain the discharge also increase (Figure 11). As shown in Figure 11b, a point is reached where the field in the sheaths becomes larger than the DC breakdown field of the background gas. At that point secondary electrons can trigger ionisation avalanches and the discharge transitions to the γ mode. Therefore, for a given RF excitation frequency and for small enough discharges, the γ mode is the only possible mode of operation.

EEPF in DBDs

The EEPF in a DBD microdischarge operated at ≈166 kHz is shown in Figure 12. The discharge is sustained in a Ne/Xe mixture at 300 Torr (39.9 kPa). The Xe concentration is 5% and the discharge configuration corresponds to a parallel plate reactor with electrodes covered with 30 μm dielectrics ($\varepsilon_r = 10$). The distance between the two parallel electrodes is 200 μm, and the discharge is driven by 200 V/3 μs bipolar square pulses with rising and falling times of 50 ns. The driving voltage is applied to the left electrode while the right one is kept grounded. Simulations are run for several consecutive pulses to accurately take into account the residual surface charges from previous pulses.

Figure 12 shows the density and potential profiles at various times after the ignition of the discharge. Initially, residual electrons in the discharge gap are accelerated against the temporary anode to generate a weak plasma near the anode (Figure 12c). As time progresses, ions strike on the cathode dielectric and secondary electrons ignite the main discharge, which has a higher density and forms closer to the cathode. As charges accumulate on the dielectrics, the voltage across the discharge gap decreases and eventually the discharge extinguishes (Figure 12a,b). The maximum plasma density is observed at ≈120 ns after each driving pulse and the voltage across the discharge gap reduces to less than 50 V in 200 ns. Although the applied voltage is 200 V, the voltage across the discharge reaches ≈375 V at ≈50 ns because of the contribution of residual charges on the dielectric surfaces from previous pulses.

The evolution of the EEPF is shown in Figure 13. In this case, the transient nature of the DBD discharge complicates the analysis. As in the previous discharges, high-energy electrons are generated in the cathode sheath and do not penetrate too deeply into the bulk plasma ($\lambda_\varepsilon \approx 10$ μm $\ll L \approx 200$ μm). The knees in the EEPF at ≈8 eV (Figure 13) are due to the same underlying principles as those in the DC and RF discharges, i.e., the faster energy relaxation for electrons with energy above the excitation threshold ($\varepsilon < \varepsilon_{ex} \approx 8$ eV for Xe).

The EEPF in the low and mid-energy range, however, differs from those in the DC and RF discharges. An additional knee is observed at ≈4 eV in the EEPF of the DBD discharge, and the low-energy electrons have a higher

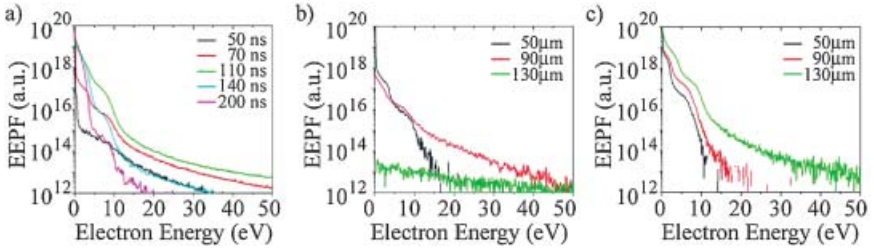

Figure 13. a) Time evolution of the EEPF in a Ne/Xe(5%) DBD discharge. EEPF at various locations measured at b) $t = 70$ ns and c) $t = 110$ ns. The distances are measured from the left hand side electrode (temporary anode).

DOI: 10.1002/ppap.200700162

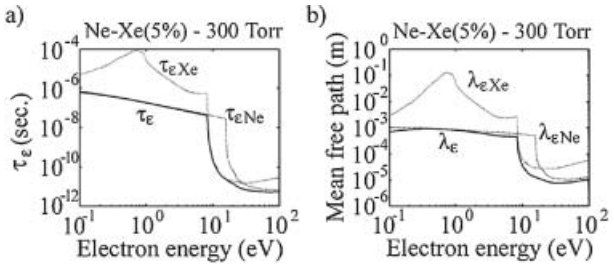

Figure 14. Electron energy relaxation time (a) and mean free path (b) in a 300 Torr (40 kPa) Ne/Xe(5%) mixture.

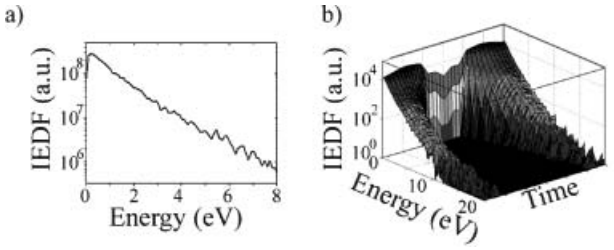

Figure 15. Energy distribution function of He^+ ions impinging on the electrode of a) 200 μm DC, and b) 100 μm RF microdischarges at atmospheric pressure. The average ion energy is $T_i = 1–3$ eV.

temperature and are less abundant than in previous discharges. The ≈4 eV threshold corresponds to the confining potential on the temporary anode (not appreciable in Figure 12 because of the large scale of the figure). Electrons below the confining potential are more abundant that those above it since they cannot reach the dielectric surface. The higher temperature of the low-energy electrons in the DBD discharge as compared to the DC and RF cases is a result of the non-locality of the electrons and the short duration of the discharge compared to the energy relaxation time (Figure 14).

Plasma/Surface Interaction: Charged Particle Fluxes

While particle kinetics in the discharge volume are important for determining reactions in the gas phase, the kinetics of particles that arrive at the electrodes play a key role in the plasma-surface interaction. In low pressure discharges, ions are accelerated in the sheaths and strike the surfaces with significant energy. As a result, the plasma process can be engineered to either sputter the target material or to activate chemical reactions. Control over the energy and flux of charged particles to the walls has enabled the use of plasmas for fabrication processes.[1] At atmospheric pressure, however, collisions limit the energy ions can acquire as they transit the sheath. While the limitation of the ion energy has the benefit of minimizing electrode erosion, collisions may actually prevent ion-induced activation of the surfaces and, therefore, limit the applicability of atmospheric pressure discharges. Figure 15 shows the energy distribution function of ions striking the electrodes of DC and RF He microdischarges at atmospheric pressure. For the RF case, the ion energy distribution function (IEDF) is time modulated because the ions can transit the sheaths in a fraction of the RF period. Despite the fact that the sheath voltage is 200–400 V, the average ion energy is 1–3 eV in both cases.

In discharges with gas mixtures, ions of low concentration substances can reach significantly higher energies owing to the unlikelihood of charge exchange resonant collisions with the background gas.[59] For example, in a 300 Torr Ne/Xe(5%) DBD discharge, the ion energy probability function of Xe^+ ions presents a high energy tail of ≈15 eV (Figure 16a), whereas Ne^+ ions have a high energy tail of only ≈4 eV. The lower temperature observed at low ion energies is attributed to the temporal evolution of the electric field in the sheath (Figure 16b), the increase of the ion/neutral collision cross section at low energies, and ionisation within the cathode sheath.[82]

Microdischarges, however, can realise an interesting new plasma-surface paradigm.[156,180] When the width of the sheaths becomes comparable to the size of the discharge gap, energetic electrons accelerated across the sheaths can reach the opposite electrode with significant energy. This is shown in Figure 17. The energy distribution function of the electrons arriving at the electrode of the RF microdischarges described in a previous section has a pronounced high-energy tail that grows as the gap size is reduced. As summarised in the table accompanying Figure 17, the mean energy of the electron flux that reaches the electrode increases as the gap size is reduced, and up to ≈50% of the total electron flux may be composed of electrons with energy above 5 eV. Since most chemical bonds have energies of a few eV, the electron flux can provide a means to activate surface chemistry in atmospheric pressure discharges. It should be noted that while a

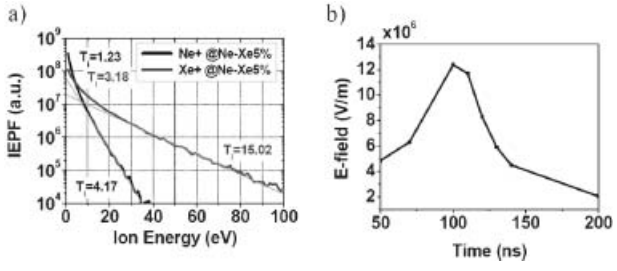

Figure 16. a) Time-integrated ion energy probability function of Ne^+ and Xe^+ ions impinging on the dielectric surface. b) Evolution of electric field in the cathode sheath for a 300 Torr Ne/Xe(5%) DBD discharge.

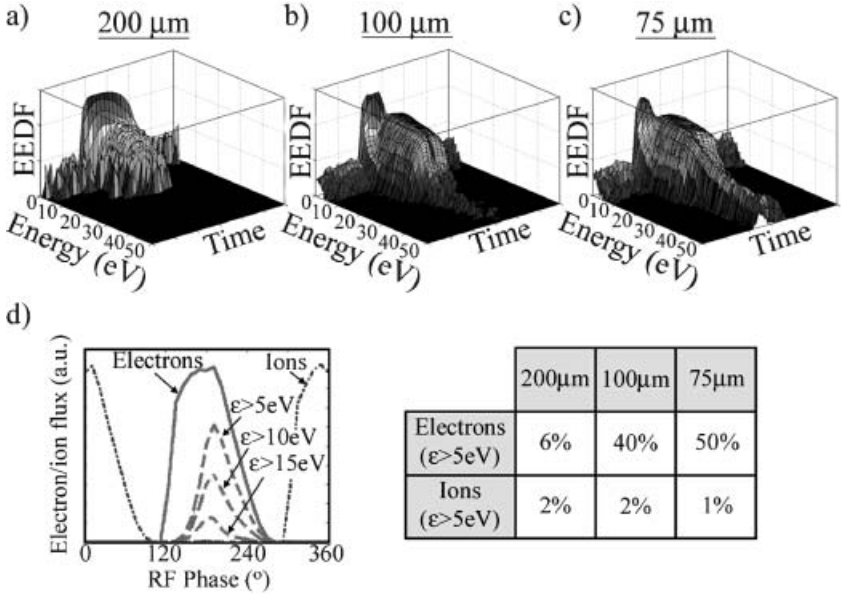

Figure 17. Time resolved energy distribution function of electrons arriving at the left hand side electrode of the RF microplasmas described in the text:[165,180] a) 200, b) 100, and c) 75 μm discharges. d) Electron and ion fluxes to the left hand side electrode as a function of time for the 100 μm microdischarge. The table displays the time-averaged percentage of energetic particles striking the electrode for 200, 100, and 75 μm discharges. Figure reprinted with permission from ref.[165]. Copyright 2007 American Physical Society.

flux of energetic electrons is also present in low-pressure discharges, the relative number of energetic electrons is smaller than that at atmospheric pressure and the energy transferred by the electrons ($\approx T_e$) is typically negligible when compared with the energy delivered by ions ($\approx V_{sheath}$). Atmospheric pressure microdischarges, however, have the opposite situation, and electrons are found to deliver more than ten times the energy delivered by ions (see table accompanying Figure 17).

As mentioned in the introduction, electrode erosion is the main cause of degradation of microplasma sources. In order to study this degradation the energy of the particles striking the electrode as well as their incidence angle is required. Limited experimental data exist in this regard, and kinetic simulations provide a valuable alternative tool to obtain such information. The electrode erosion profile can be calculated by combining the ion flux obtained from the plasma simulation with the energy and angle dependent sputtering yield obtained either experimentally or computationally (e.g., SRIM[182]).

Reasonable agreement can be found between erosion profiles predicted by simulation and those observed in experiments. As an example, the erosion profile of a microhollow cathode is shown in Figure 18. As observed experimentally,[3] the entrance and the centre of the hollow cathode are the regions most affected by the ion bombardment. These are the regions that receive the largest influx of ions. It should be noted, however, that the erosion profile is not directly proportional to the flux since the sputtering yield depends on the energy and incidence angle of the bombarding particle (Figure 18). Good agreement between simulation and experimental observations was also reported in regard to the erosion profile of MgO layers in plasma display panel cells.[59]

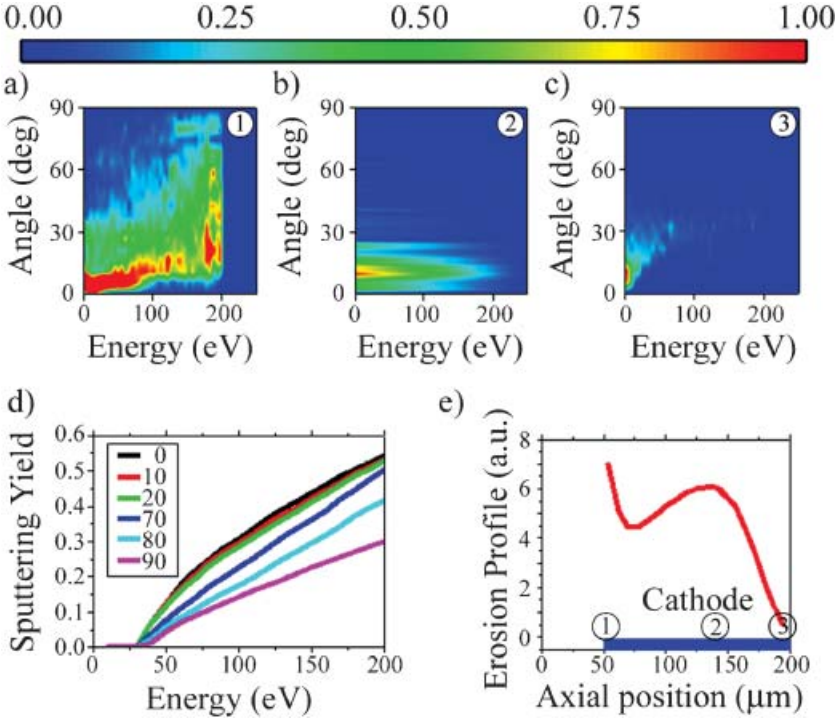

Figure 18. Erosion profile in a microhollow cathode discharge. a–c) Energy and angle distribution of ions impinging onto the three different regions of the cathode shown in (e). d) Sputtering yield of Mo by Ar^+ ions. e) Erosion profile. The incidence angle is measured with respect to the cathode surface normal, i.e., an ion impinging perpendicularly to the surface has an incidence angle of 0 degrees.

DOI: 10.1002/ppap.200700162

Microplasmas for Biomedical Applications

It is evident from their particle kinetics that microplasmas are particularly effective in producing large fluxes of reactive plasma species and energetic charged particles at low gas temperatures, often close to room temperature. This highly non-equilibrium character is desirable for a very wide range of applications as discussed in the introduction section. With considerable progress made over the past 10 years or so, biomedical applications of microplasmas are an excellent example of their immense practical potential. From the standpoint of fundamental science, the impact of microplasmas upon biology and medicine is inevitable as they provide a rich environment of charged particles, reactive ground-state species, excited species and metastables, UV photons, and intense electric fields, any of which can in principle significantly affect bacterial and mammalian cells. As a result, microplasmas can be developed for beneficial use in biology and medicine.

Perhaps most studied and also most comprehensively established is the outstanding capability of microplasmas to inactivate microorganisms and destroy biomolecules. Since the first group of feasibility studies in the second half of the 1990s,[183–187] atmospheric microplasmas have been shown to inactivate a very wide spectrum of microorganisms including spores, Gram-negative bacteria, Gram-positive bacteria, biofilm-forming microorganisms, yeast, mould, mycobacterium, and viruses.[188] As a result, the bactericidal properties of microplasmas have been well established and future studies of microplasma inactivation are likely to support this further with a longer list of microorganisms that are susceptible to microplasma treatment. Significantly, the bactericidal ability of microplasmas has been comprehensively established against some of the most deadly or/and most resistive microorganisms such as *Bacillus subtilis*, *Escherichia coli* (K12 and O157), *Staphylococcus aureus*, and *Candida albicans*.[183–201] These data highlight a real and significant opportunity for microplasmas to be developed as a medical decontamination technology to address contamination of surgical instruments, medical devices, and hospital wards. A key challenge for the microplasma technology to reach widespread use in medical sterilisation lies in the translation of its fundamental bactericidal properties into effective decontamination systems as well as the associated engineering tasks, given the vast variety in materials, shapes, and configurations employed for medical instruments and devices.

Another critical challenge stems from the fact that the majority of medical contamination is not only by microorganisms but also biomolecules such as proteins, DNA, and lipids. The obvious example is the contamination of the mis-folded prion proteins, widely regarded as the etiologic agent of spongiform neurodegenerative pathologies such as bovine spongiform encephalopathy (BSE), scrapie, and Creutzfeldt-Jakob diseases (CJD).[202] Prion proteins are resistant to all current sterilisation strategies including autoclaving, ionizing radiation, ethylene oxide, and formaldehyde,[203] and as a result have forced the unsustainably expensive option of single-use surgical instruments. For microplasma technology to become a universally applicable sterilisation solution, it is highly desirable that its biocidal properties could also achieve protein removal and destruction. Very recent studies suggest that microplasmas are also capable of protein destruction.[12,204] While microplasma protein destruction is a relatively new angle of investigation and much more needs to be studied, the prospect of a microplasma-based medical sterilisation technology is real and highly encouraging. It is worth emphasizing that the current review of plasma decontamination studies are largely restricted to atmospheric microplasmas and that similar success of medical decontamination has also been achieved with low-pressure plasmas.[205–210] The parallel development of a vacuum-plasma sterilisation technology offers valuable contrast and similarity with which to compare and advance the atmospheric microplasma technology for medical decontamination.

The generic biocidal properties of microplasmas can in principle be used for biological decontamination other than sterilisation of surgical instruments and medical devices. One example is food decontamination, and this line of research has benefited from the success of microplasma inactivation of biofilm-forming bacteria.[211,212] More recently, microplasmas have been shown to effectively inactivate spoilage microorganisms, such as *Saccharomyces cerevisae*, *Pantoea agglomerans*, and *Gluconacetobacter liquefaciens*, on both abiotic surfaces and fruit surfaces.[213,214] The ability of microplasmas to destroy bacteria embedded in a growing biofilm, a three-dimensional exopolysaccharide matrix, is also significant for treating dental caries.[215] With a similar drive to enable real benefits, atmospheric microplasmas have recently been used to attempt inactivation of bacteria on living tissues and wounds.[216,217] This is an exciting development of microplasma research that can bring profound benefits to medicine.

While the field of microplasma decontamination is expanding into different applications, increasing attention is now being directed to understanding the mechanisms of microplasma inactivation. At present, these are yet to be conclusively established despite considerable efforts.[188] For atmospheric plasmas, it has commonly been believed that reactive plasma species, such as ground and excited state oxygen atoms, hydroxyl radicals, ozone, and nitride oxides, are important, whilst UV photons play a relatively minor role.[188,218] Further discrimination of roles of

different plasma species is challenging, because it is difficult to isolate the effect of one particular plasma species by suppressing the production of other possible biocidal plasma species. An additional challenge is to access established experimental techniques that can measure the absolute concentrations of relevant plasma species. While these difficulties are at present being addressed using methodologies that are essentially plasma-physics based, it is possible to go beyond the boundary of plasma physics and seek techniques developed for other disciplines. One such example is the use of *E. coli* mutants not as contaminants but as sensors of oxygen plasma species thus providing an additional line of information in the current quest for a full understanding of microplasma decontamination.[219] It is worth mentioning the importance of the studies that aim to identify and understand the biological signatures of microplasma impact.[220–224] It is conceivable that the combination of the physical mechanisms (e.g., identification and quantitative evaluation of biocidal plasma agents) and the biological mechanisms (e.g., identification and confirmation of plasma-induced biological events) will be central to the future success of microplasma decontamination.

Finally, the scope of microplasmas for biomedical applications goes beyond decontamination and sterilisation. For example, microplasmas have been used for blood coagulation[217,225] and tissue ablation[226] in surgery, DNA extraction,[227] apoptosis induction of cancer cells,[9,228] cell manipulation for cell adhesion control[229] and DNA transfection,[230] and more recently wound healing.[216] These are at varying stages of their development, each of which can benefit significantly from a fundamental understanding of particle kinetics of microplasmas and each of which offers stimuli to the advancement of fundamental microplasma science.

Conclusion and Outlook

Microplasmas are small discharges with dimensions that range from a few micrometers up to a few millimetres. These microdischarges have large surface-to-volume ratios that favour large electric fields and large spatial gradients. These characteristics allow microplasmas to depart from thermodynamic equilibrium even when driven at input power levels of $MW \cdot cm^{-3}$. Because of the reactivity, low-gas temperature, non-equilibrium character, and portability, microplasmas have potential application in many scientific disciplines. The potential economic and technological impact of microplasmas has drawn the attention of many researchers, and a large variety of microplasmas can be found in the literature. A review of the most popular DC, AC, RF, and microwave microplasmas sources has been presented in this manuscript.

While interest in microplasmas was first driven by their potential application, there is no doubt that microplasmas represent a new realm of plasma physics. While similarities can be found between microplasmas and the more conventional low-pressure large-scale plasmas, microplasmas have distinct characteristics. In order to unravel the underlying physics governing these discharges, particle kinetics must be understood. To that end, electron and ion kinetics in various microplasma discharges have been discussed. It is concluded that, in general, the electron energy distribution function is far from thermodynamic equilibrium and that despite the high pressure at which microplasmas are typically operated, non-local electron kinetics can be important. These conclusions should trigger the kinetic study of high pressure microdischarges, a topic that until now has been dominated by hydrodynamic studies.

As a result of the potential application of microplasmas in a broad range of scientific fields, research on microplasmas is expected to continue growing in the coming years. Microplasmas are no longer a laboratory curiosity, and research groups should work jointly on different aspects of generation, diagnostics, modelling, and applications of microplasmas. As our understanding of the discharges deepens and the control over the discharge characteristics grows, more efficient devices and more challenging tasks will be addressed. A current trend has shifted the interest in microplasmas towards environmental and biomedical applications. An outlook of biomedical applications of plasmas has been presented in this manuscript as the trend is expected to continue in the future. In particular, considerable progress has been made in advancing microplasma technology for the inactivation of microorganisms and biomolecules. This well-established biocidal capability is being translated into sterilisation and disinfection systems specifically catered towards medical sterilisation and food decontamination. In parallel, growing interests have been directed to the fundamental question of the character and nature of plasma interaction with bacteria and biomolecules. There is a significant and obvious scope for the application-focused research and the curiosity driven research to overlap and interplay. The success of microplasma decontamination is likely to provide stimuli and confidence in the pursuit of other biomedical applications of microplasmas.

Acknowledgements: This work was supported in part by the *Korean Ministry of Education* through the Brain Korea 21 program and the *Korean Science and Engineering Foundation* under Grant No. R01-2007-000-10730-0, and in part by the *Engineering and Physical Science Research Council*, UK under Grant EP/D034825.

DOI: 10.1002/ppap.200700162

Received: November 21, 2007; Accepted: January 10, 2008; DOI: 10.1002/ppap.200700162

Keywords: biomedical; electron-energy distribution function (EEDF); ion-energy distribution function (IEDF); microdischarges; microplasmas

[1] M. A. Lieberman, A. J. Lichtenberg, "*Principles of Plasma Discharges*", John Wiley & Sons Inc., New Jersey 2005.
[2] "*Plasma Science: Advancing Knowledge in the National Interest*" National Academies report, National Academies Press, Washington D. C 2007.
[3] A. D. White, *J. Appl. Phys.* **1959**, *30*, 711.
[4] K. H. Becker, K. H. Schoenbach, J. G. Eden, *J. Phys. D: Appl. Phys.* **2006**, *39*, R55.
[5] K. Tachibana, *IEEJ Trans.* **2006**, *1*, 145.
[6] V. Karanassios, *Spectrochim. Acta B* **2004**, *59*, 909.
[7] R. Foest, M. Schmidt, K. Becker, *Int. J. Mass Spectrom.* **2005**, *248*, 87.
[8] M. Miclea, J. Franzke, *Plasma Chem. Plasma Proc.* **2007**, *27*, 205.
[9] Hyogo, Japan (2002); Hoboken, NJ (2004); Greifswald, Germany (2006); Tainan City, Taiwan (2007) http://www.iwm2007.org.tw.
[10] I. E. Kieft, M. Kurdi, E. Stoffels, *IEEE Trans. Plasma Sci.* **2006**, *34*, 1331.
[11] M. Laroussi, C. Tendero, X. Lu, S. Alla, W. L. Hynes, *Plasma Proc. Polym.* **2006**, *3*, 470.
[12] X. T. Deng, J. J. Shi, M. G. Kong, *J. Appl. Phys.* **2007**, *101*, 074701.
[13] G. Fridman, A. Shereshevsky, M. M. Jost, A. D. Brooks, A. Fridman, A. Gutsol, V. Vasilets, G. Friedman, *Plasma Chem. Plasma Proc.* **2007**, *27*, 163.
[14] K. Becker, A. Koutsospyros, S.-M. Yin, C. Christodoulatos, N. Abramzon, J. C. Joaquin, G. Brelles-Mariño, *Plasma Phys. Controlled Fusion* **2005**, *47*, B513.
[15] R. Rahul, O. Stan, A. Rahman, E. Littlefield, K. Hoshimiya, A. P. Yalin, A. Sharma, A. Pruden, C. A. Moore, Z. Yu, G. J. Collins, *J. Phys. D: Appl. Phys.* **2005**, *38*, 1750.
[16] J. P. Boeuf, *J. Physics D: Appl. Phys.* **2003**, *36*, R53.
[17] J. G. Eden, S. J. Park, *Phys. Plasmas* **2006**, *13*, 057101.
[18] K. H. Schoenbach, A. El-Habachi, M. M. Moselhy, W. Shi, R. H. Stark, *Phys. Plasmas* **2000**, *7*, 2186.
[19] P. Kurunczi, J. Lopez, H. Shah, K. Becker, *Int. J. Mass Spectrom.* **2001**, *205*, 277.
[20] A. Kono, J. Wang, M. Aramaki, *Thin Solid Films* **2006**, *506*, 444.
[21] D. Janasek, J. Franzke, A. Manz, *Nature* **2006** *442*, 374.
[22] M. Miclea, K. Kunze, U. Heitmann, S. Florek, J. Franzke, K. Niemax, *J. Phys. D: Appl. Phys.* **2005**, *38*, 1709.
[23] P. Siebert, G. Petzold, A. Hellenbart, J. Müller, *Appl. Phys. A* **1998**, *67*, 155.
[24] J. Hopwood, *J. Microelectromech. Systems* **2000**, *9*, 309.
[25] N. P. Ostrom, J. G. Eden, *Appl. Phys. Lett.* **2005**, *87*, 141101.
[26] P. von Allmen, D. J. Sadler, C. Jensen, N. P. Ostrom, S. T. McCain, B. A. Vojak, J. G. Eden, *Appl. Phys. Lett.* **2003**, *82*, 4447.
[27] R. H. Stark, K. H. Schoenbach, *Appl. Phys. Lett.* **1999**, *74*, 3770.
[28] O. Sakai, T. Sakaguchi, K. Tachibana, *Appl. Phys. Lett.* **2005**, *87*, 241505.
[29] O. Sakai, T. Sakaguchi, K. Tachibana, *Plasma Phys. Controlled Fusion* **2005**, *47*, B617.
[30] R. M. Sankaran, D. Holunga, R. C. Flagan, K. P. Giapis, *Nano Lett.* **2005**, *5*, 537.
[31] R. M. Sankaran, K. P. Giapis, *Appl. Phys. Lett.* **2001**, *79*, 593.
[32] D. D. Hsu, D. B. Graves, *J. Phys. D: Appl. Phys.* **2003**, *36*, 2898.
[33] D. D. Hsu, D. B. Graves, *Plasma Chem. Plasma Process.* **2005**, *25*, 1.
[34] R. A. Arakoni, A. N. Bhoj, M. J. Kushner, *J. Phys. D: Appl. Phys.* **2007**, *40*, 2476.
[35] Y. Takao, K. Ono, *Plasma Sources Sci. Technol.* **2006**, *15*, 211.
[36] R. A. Arakoni, J. J. Ewing, M. J. Kushner, *33rd IEEE International Conference on Plasma Science*, Traverse City, MI, June 2006.
[37] P. S. Kothnur, L. L. Raja, *J. Appl. Phys.* **2005**, *97*, 043305.
[38] E. Moreau, C. Louste, G. Artana, M. Forte, G. Touchard, *Plasma Process. Polym.* **2006**, *3*, 697.
[39] J. R. Roth, D. M. Sherman, S. P. Wilkinson, *AIAA J.* **2000**, *38*, 1166.
[40] R. M. Sankaran, K. P. Giapis, *J. Phys. D: Appl. Phys.* **2003**, *36*, 2914.
[41] C. G. Wilson, Y. B. Gianchandani, *J. Microelectromech. Syst.* **2001**, *10*, 50.
[42] T. Ichiki, R. Tauro, Y. Horiike, *J. Appl. Phys.* **2004**, *95*, 35.
[43] Y. Shimizu, T. Sasaki, T. Ito, K. Terashima, N. Koshizaki, *J. Phys. D: Appl. Phys.* **2003**, *36*, 2940.
[44] J. Benedikt, K. Focke, A. Yanguas-Gil, A. von Keudell, *Appl. Phys. Lett.* **2006**, *89*, 251504.
[45] A. Koutsospyros, S.-Y. Yin, C. Christodoulatos, K. Becker, *IEEE Trans. Plasma Sci.* **2005**, *33*, 42.
[46] O. Minayeva, J. Hopwood, *J. Anal. At. Spectrom.* **2003**, *18*, 856.
[47] J. Hopwood, F. Iza, *J. Anal. At. Spectrom.* **2004**, 1145.
[48] M. Sawada, T. Tomai, T. Ito, H. Fujiwara, K. Terashima, *J. Appl. Phys.* **2006**, *100*, 123304.
[49] E. H. Lock, A. V. Saveliev, L. A. Kennedy, *IEEE Trans. Plasma Sci.* **2005**, *33*, 850.
[50] http://verionix.com
[51] F. Iza, J. K. Lee, *Comput. Phys. Commun.* **2007**, *177*, 72.
[52] H. Fujiyama, *Surf. Coat. Technol.* **2000**, *131*, 278.
[53] F. Iza, J. Hopwood, *Plasma Sources Sci. Technol.* **2002**, *11*, 229.
[54] J. C. T. Eijkel, H. Stoeri, A. Manz, *Anal. Chem.* **1999**, *71*, 2600.
[55] J. C. T. Eijkel, H. Stoeri, A. Manz, *Anal. Chem.* **2000**, *72*, 2547.
[56] J. Choi, F. Iza, J. K. Lee, *IEEE Trans. Plasma Sci.* **2007**, *37*, 1274.
[57] T. Ito, M. Cappelli, *Phys. Rev. E* **2006**, *73*, 046401.
[58] R. Hippler, H. Kersten, M. Schmidt, K. H. Schoenbach, "*Low Temperature Plasmas: Fundamentals, Technologies, and Techniques*", 2nd edition, Wiley-VCH, Weinheim 2007.
[59] S. M. Lee, S. S. Yang, Y. S. Seo, J. K. Lee, *Plasma Chem. Plasma Process.* **2007**, *27*, 349.
[60] F. Iza, J. A. Hopwood, *Plasma Sources Sci. Technol.* **2005**, *14*, 397.
[61] J. Hopwood, F. Iza, S. Coy, D. B. Fenner, *J. Phys. D: Appl. Phys.* **2005**, *38*, 1698.
[62] R. H. Stark, K. H. Schoenbach, *Appl. Phys. Lett.* **1999**, *74*, 3770.
[63] F. Iza, J. A. Hopwood, *IEEE Trans. Plasma Sci.* **2003**, *31*, 782.
[64] J. L. Walsh, J. J. Shi, M. G. Kong, *Appl. Phys. Lett.* **2006**, *88*, 3.
[65] F. Iza, J. A. Hopwood, *IEEE Trans. Plasma Sci.* **2005**, *33*, 306.
[66] I. Muller, C. Punset, E. Ammelt, H.-G. Purwins, J. P. Boeuf, *IEEE Trans. Plasma Sci.* **1999**, *27*, 20.
[67] N. Takano, K. H. Schoenbach, *Plasma Sources Sci. Technol.* **2006**, *15*, S109.
[68] M. S. Benilov, *Plasma Sources Sci. Technol.* **2007**, *16*, 422.

[69] J. W. Frame, D. J. Wheeler, T. A. DeTemple, J. G. Eden, *Appl. Phys. Lett.* **1997**, *71*, 1165.
[70] S. J. Park, J. Chen, C. Liu, J. G. Eden, *Appl. Phys. Lett.* **2001**, *78*, 419.
[71] M. Moselhy, K. H. Schoenbach, *J. Appl. Phys.* **2004**, *95*, 1642.
[72] F. Adler, E. Davliatchine, E. Kindel, *J. Phys. D: Appl. Phys.* **2002**, *35*, 2291.
[73] R. Gomer, "*Field Emission and Field Ionization*", American Institute of Physics, Washington DC 1993.
[74] M. Radmilovic-Radjenovic, J. K. Lee, F. Iza, G. Y. Park, *J. Phys. D: Appl. Phys.* **2005**, *38*, 950.
[75] E. Hourdakis, G. W. Bryant, N. M. Zimmerman, *J. Appl. Phys.* **2006**, *100*, 123306.
[76] W. F. Gale, T. C. Totemeier, "*Smithells Metals Reference Book*", 8th edition, Elsevier New York, **2004**.
[77] W. S. Boyle, P. Kisliuk, *Phys. Rev.* **1995**, *97*, 255.
[78] J. M. Bonard, H. Kind, T. Stockli, L. O. Nilsson, *Solid State Electron.* **2001**, *45*, 893.
[79] C. G. Wilson, Y. B. Gianchandani, *IEEE Trans. Electron. Devices* **2002**, *49*, 2317.
[80] L. L. Raja, P. L. Varghese, D. E. Wilson, *AIAA J. Thermophys. Heat Transfer* **1997**, *11*, 353.
[81] S. J. Park, J. G. Eden, K. H. Park, *Appl. Phys. Lett.* **2004**, *84*, 4481.
[82] G. J. Kim, F. Iza, J. K. Lee, *J. Phys. D: Appl. Phys.* **2006**, *39*, 4386.
[83] M. Moselhy, I. Petzenhauser, K. Frank, K. H. Schoenbach, *J. Phys. D: Appl. Phys.* **2003**, *36*, 2922.
[84] R. H. Stark, K. H. Schoenbach, *J. Appl. Phys.* **2001**, *89*, 3568.
[85] P. Gill, C. E. Webb, *J. Phys. D: Appl. Phys.* **1977**, *10*, 299.
[86] J. Mizeraczyk, W. Urbanik, *J. Phys. D: Appl. Phys.* **1983**, *16*, 2119.
[87] M. J. Kushner, *J. Appl. Phys.* **2004**, *95*, 846.
[88] S. J. Park, K. F. Chen, N. P. Ostrom, J. G. Eden, *Appl. Phys. Lett.* **2005**, *86*, 111501.
[89] K. F. Chen, N. P. Ostrom, S. J. Park, J. G. Eden, *Appl. Phys. Lett.* **2006**, *88*, 061121.
[90] K. H. Becker, U. Kogelschatz, K. H. Schoenbach, R. J. Barker, Eds., "*Non-Equilibrium Air Plasmas at Atmospheric Pressure*", IOP Publishing Ltd., Bristol 2005.
[91] M. Miclea, K. Kunze, G. Musa, J. Franzke, K. Niemax, *Spectrochim. Acta B* **2001**, *56*, 37.
[92] O. Sakai, Y. Kishimoto, K. Tachibana, *J. Phys. D: Appl. Phys.* **2005**, *38*, 431.
[93] M. Teschke, J. Kedzierski, E. G. Finantu-Dinu, D. Korzec, J. Engemann, *IEEE Trans. Plasma Sci.* **2005**, *33*, 310.
[94] J. Guikema, N. Miller, J. Niehof, M. Klein, M. Walhout, *Phys. Rev. Lett.* **2000**, *85*, 3817.
[95] L. Dong, F. Liu, S. Liu, Y. He, W. Fan, *Phys. Rev. E* **2005**, *72*, 046215.
[96] U. Kogelschatz, *Plasma Chem. Plasma Process.* **2003**, *23*, 1.
[97] M. Klein, N. Miller, M. Walhout, *Phys. Rev. E* **2001**, *64*, 026402.
[98] F. Massines, A. Rabechi, P. Decomps, R. B. Gadri, P. Segur, C. Mayoux, *J. Appl. Phys.* **1998**, *83*, 2950.
[99] A. S. Chiper, V. Anit, C. Agheorghiesei, V. Pohoat, M. Anit, G. Popa, *Plasma Process. Polym.* **2004**, *1*, 57.
[100] G. Nersisyan, W. G. Graham, *Plasma Sources Sci. Technol.* **2004**, *13*, 582.
[101] Y. B. Golubovskii, V. A. Maiorov, J. Behnke, J. F. Behnke, *Plasma Process. Polym.* **2005**, *2*, 188.
[102] S. Cany, J. Kang, C. Punset, J. P. Boeuf, "Efficiency of Radiofrequency Excited Plasma-Displays Cells. Model Predictions", in: *Proc. International Display Workshop 1999 (IDW'99)*, PDPp4-1, pp. 751–754.
[103] S. Y. Moon, W. Choe, B. K. Kang, *Appl. Phys. Lett.* **2004**, *84*, 188.
[104] J. J. Shi, D. W. Liu, M. G. Kong, *Appl. Phys. Lett.* **2006**, *89*, 3.
[105] J. J. Shi, D. W. Liu, M. G. Kong, *IEEE Trans. Plasma Sci.* **2007**, *35*, 137.
[106] J. J. Shi, M. G. Kong, *Appl. Phys. Lett.* **2007**, *90*, 111502.
[107] M. Laroussi, A. Alexeff, J. P. Richardson, F. F. Dyer, *IEEE Trans. Plasma Sci.* **2002**, *30*, 158.
[108] X. P. Lu, M. Laroussi, *J. Appl. Phys.* **2006**, *100*, 063302.
[109] M. Miclea, K. Kunze, J. Franze, K. Niemax, *J. Anal. At. Spectrom.* **2004**, *19*, 990.
[110] A. Fridman, A. Chirokov, A. Gutsol, *J. Phys. D: Appl. Phys.* **2005**, *38*, R1.
[111] D. B. Kim, J. K. Rhee, S. Y. Moon, W. Choe, *Thin Solid Films* **2007**, *515*, 4913.
[112] Y. Sakiyama, D. B. Graves, *J. Phys. D: Appl. Phys.* **2006**, *39*, 3644.
[113] Y. Sakiyama, D. B. Graves, *J. Appl. Phys.* **2007**, *101*, 073306.
[114] Z. Q. Yu, K. Hoshimiya, J. D. Williams, S. F. Polvinen, G. J. Collins, *Appl. Phys. Lett.* **2003**, *83*, 854.
[115] E. Stoffels, A. J. Flikweert, W. W. Stoffels, G. M. W. Kroesen, *Plasma Sources Sci. Technol.* **2002**, *11*, 383.
[116] Y. C. Hong, S. C. Cho, H. S. Uhm, *Appl. Phys. Lett.* **2007**, *90*, 141501.
[117] H. Yoshiki, K. Taniguchi, Y. Horiike, *Jpn. J. Appl. Phys.* **2002**, *41*, 5797.
[118] K. Takaki, H. Kirihara, C. Noda, S. Mukaigawa, T. Fujiwara, *Plasma Process. Polym.* **2006**, *3*, 734.
[119] A. Schutze, J. Y. Jeong, S. E. Babayan, J. Park, G. S. Selwyn, R. F. Hicks, *IEEE Trans. Plasma Sci.* **1998**, *26*, 1685.
[120] J. J. Shi, X. T. Deng, R. Hall, J. P. Punnett, M. G. Kong, *J. Appl. Phys.* **2003**, *94*, 06303.
[121] A. Bass, C. Chevalier, M. W. Blades, *J. Anal. At. Spectrom.* **2001**, *16*, 919.
[122] H. Yoshiki, Y. Horiike, *Jpn. J. Appl. Phys. II* **2001**, *40*, L360.
[123] D. W. Liu, J. J. Shi, M. G. Kong, *Appl. Phys. Lett.* **2007**, *90*, 041502.
[124] A. Bass, C. Chevalier, M. W. Blades, *J. Anal. At. Spectrom.* **2001**, *16*, 919.
[125] M. Moravej, R. F. Hicks, *Chemical Vapor Deposition* **2005**, *11*, 469.
[126] K. Taniguchi, T. Fukasawa, H. Yoshiki, Y. Horiike, *Jpn. J. Appl. Phys.* **2003**, *42*, 6584.
[127] A. Schütze, J. Y. Jeong, S. E. Babayan, J. Park, G. S. Selwyn, R. F. Hicks, *IEEE Trans. Plasma Sci.* **1998**, *26*, 1685.
[128] J. J. Shi, M. G. Kong, *J. Appl. Phys.* **2003**, *94*, 6303.
[129] X. Yang, M. Moravej, G. R. Nowling, S. E. Babayan, J. Penelon, J. P. Chang, R. F. Hicks, *Plasma Sources Sci. Technol.* **2005**, *14*, 314.
[130] S. Y. Moon, B. K. Kang, W. Choe, *Phys. Plasmas* **2006**, *13*, 033502.
[131] J. Park, I. Henins, H. W. Herrmann, G. S. Selwyn, *J. Appl. Phys.* **2001**, *89*, 15.
[132] M. Surendra, D. B. Graves, *Appl. Phys. Lett.* **1991**, *59*, 2091.
[133] S. K. Ahn, S. J. You, H. Y. Chang, *Appl. Phys. Lett.* **2006**, *89*, 161506.
[134] Y. Yin, J. Messier, J. Hopwood, *IEEE Trans. Plasma Sci.* **1999**, *27*, 1516.
[135] T. Ito, K. Terashima, *Appl. Phys. Lett.* **2002**, *80*, 2648.
[136] T. Ichiki, *Plasma Sources Sci. Technol.* **2003**, *12*, S16.
[137] F. Iza, J. Hopwood, *Plasma Sources Sci. Technol.* **2002**, *11*, 229.
[138] Y. Yin, J. Messier, J. Hopwood, *IEEE Trans. Plasma Sci.* **1999**, *27*, 5.

DOI: 10.1002/ppap.200700162

[139] J. Hopwood, O. Minayeva, Y. Yin, *J. Vac. Sci. Technol. B* **2000**, *18*, 2446.
[140] J. Hopwood, F. Iza, *J. Anal. At. Spectrom.* **2004**, *19*, 1145.
[141] A. M. Bilgic, U. Engel, E. Voges, M. Kuckelheim, J. A. C. Broekaer, *Plasma Sources Sci. Technol.* **2000**, *9*, 1.
[142] A. M. Bilgic, E. Voges, U. Engel, J. A. C. Broekaert, *J. Anal. At. Spectrom.* **2000**, *15*, 579.
[143] S. Schermer, N. H. Bings, A. M. Bilgiç, R. Stonies, E. Voges, J. A. C. Broekaert, *Spectrochim. Acta B* **2003**, *58*, 1585.
[144] F. Iza, J. Hopwood, *IEEE Trans. Plasma Sci.* **2004**, *32*, 498.
[145] F. Iza, J. Hopwood, *Plasma Sources Sci. Technol.* **2005**, *14*, 397.
[146] J. Narendra, Y. Gu, J. Zhang, T. A. Grotjohn, N. Xi, J. Asmussen, *IEEE International Conference on Plasma Science*, Traverse City, MI **2006**, 202.
[147] A. Kono, T. Sugiyama, T. Goto, H. Furuhashi, Y. Uchida, *Jpn. J. Appl. Phys. II* **2001**, *40*, L238.
[148] J. Kim, K. Terashima, *Appl. Phys. Lett.* **2005**, *86*, 191504.
[149] R. Stonies, S. Schermer, E. Voges, J. A. C. Broekaert, *Plasma Sources Sci. Technol.* **2004**, *13*, 604.
[150] S. Zuo, K. Hemawan, J. J. Narendra, T. A. Grotjohn, J. Asmussen, *IEEE Conference on Plasma Science*, Baltimore MD **2004**, 310.
[151] J. Pollak, M. Moisan, Z. Zakrzewski, *Plasma Sources Sci. Technol.* **2007**, *16*, 310.
[152] K. Tachibana, K. Mizokami, N. Kosugi, T. Sakai, *IEEE Trans. Plasma Sci.* **2003**, *31*, 68.
[153] Q. Wang, I. Koleva, V. M. Donnelly, D. J. Economou, *J. Phys. D: Appl. Phys.* **2005**, *38*, 1690.
[154] J. T. Ouyang, Th. Callegari, B. Caillier, J. P. Boeuf, *J. Phys. D: Appl. Phys.* **2003**, *36*, 1959.
[155] J. K. Rhee, D. B. Kim, S. Y. Moon, W. Choe, *Thin Solid Films* **2007**, *515*, 4909.
[156] A. Kono, K. Iwamoto, *Jpn. J. Appl. Phys. II* **2004**, *43*, L1010.
[157] K. W. Whang, J. K. Kim, *IEEE Trans. Plasma Sci.* **2006**, *34*, 311.
[158] K. Niemi, S. Reuter, L. Schaper, N. Knake, V. Schulz-von der Gathen, T. Gans, *J. Phys.: Conf. Ser.* **2007**, *71*, 012012.
[159] Y. Aranda Gonzalvo, T. D. Whitmore, J. A. Rees, D. L. Seymour, E. Stoffels, *J. Vac. Sci. Technol. A* **2006**, *24*, 550.
[160] R. G. Longwitz, H. van Lintel, P. Renaud, *J. Vac. Sci. Technol. A* **2003**, *21*, 1570.
[161] J. A. Wright, R. A. Miller, E. G. Nazarov, *IEEE International Conference on Micro Electro Mechanical Systems*, Istanbul, **2006**, 378.
[162] F. Iza, S. H. Lee, J. K. Lee, "Computer Modeling of Low-Temperature Plasmas", in: *Gas Discharges: Fundamentals and Applications*, Jayr de Amorim Filho, Ed., Research Signpost, 2007.
[163] H. C. Kim, F. Iza, S. S. Yang, M. Radmilovic-Radjenovic, J. K. Lee, *J. Phys. D: Appl. Phys.* **2005**, *38*, R283.
[164] F. Iza, S. S. Yang, H. C. Kim, J. K. Lee, *J. Appl. Phys.* **2005**, *98*, 043302.
[165] F. Iza, J. K. Lee, M. G. Kong, *Phys. Rev. Lett.* **2007**, *99*, 075004.
[166] J. J. Shi, M. G. Kong, *Phys. Rev. Let.* **2006**, *96*, 105009.
[167] J. J. Shi, M. G. Kong, *J. Appl. Phys.* **2005**, *97*, 023306.
[168] Q. Wang, D. Economou, V. Donnelly, *J. Appl. Phys.* **2006**, *100*, 023301.
[169] J. P. Verboncoeur, A. B. Langdon, N. T. Gladd, *Comput. Phys. Commun.* **1995**, *87*, 199.
[170] J. P. Verboncoeur, M. V. Alves, V. Vahedi, C. K. Birdsall, *J. Comput. Phys.* **1993**, *104*, 321.
[171] S. S. Yang, S. M. Lee, F. Iza, J. K. Lee, *J. Phys D: Appl. Phys.* **2006**, *39*, 2775.
[172] G. Y. Park, S. J. You, F. Iza, J. K. Lee, *Phys. Rev. Lett.* **2007**, *98*, 085003.
[173] V. I. Kolobov, V. A. Godyak, *IEEE Trans. Plasma Sci.* **1995**, *23*, 503.
[174] H. C. Kim, J. K. Lee, *Phys. Rev. Lett.* **2004**, *93*, 085003.
[175] V. I. Kolobov, *J. Phys. D: Appl. Phys.* **2006**, *39*, R487.
[176] I. D. Kaganovich, O. V. Polomarov, C. E. Theodosiou, *IEEE Trans. Plasma Sci.* **2006**, *34*, 696.
[177] J. Choi, F. Iza, J. K. Lee, C. M. Ryu, *IEEE Trans. Plasma Sci.* **2007**, *37*, 1274.
[178] V. A. Godyak, V. P. Meytlis, H. R. Strauss, *IEEE Trans. Plasma Sci.* **1995**, *23*, 728.
[179] C. A. DeJoseph, Jr., V. I. Demidov, A. A. Kudryavtsev, *Phys. Plasmas* **2007**, *14*, 057101.
[180] F. Iza, J. K. Lee, in: *Proc. of the 18th International Symposium Plasma Chemistry*, Kyoto, Japan 2007.
[181] S. V. Berezhnoi, I. D. Kaganovich, Martin. Misina, A. Bogaerts, R. Gijbels, *IEEE Trans. Plasma Sci.* **1999**, *27*, 1339.
[182] J. F. Ziegler, J. P. Biersack, U. Littmark, "*The Stopping and Range of Ions in Solids*", Pergamon Press, New York 1985. (http://www.srim.org/.)
[183] M. Laroussi, *IEEE Trans. Plasma Sci.* **1996**, *24*, 1188.
[184] K. Kelly-Wintenberg, T. C. Montie, C. Brickman, J. R. Roth, A. K. Carr, K. Sorge, L. C. Wadsworth, P. P. Y. Tsai, *J. Ind. Microbiol. Biotechnol.* **1998**, *20*, 69.
[185] K. Kelly-Wintenberg, A. Hodge, T. C. Montie, L. Deleanu, D. Sherman, J. R. Roth, P. Tsai, L. C. Wadsworth, *J. Vac. Sci. Technol. A* **1999**, *17*, 1539.
[186] P. Koulik, S. Begounov, S. Goloviatinskii, *Plasma Chem., Plasma Process.* **1999**, *19*, 311.
[187] H. W. Herrmann, I. Henins, J. Park, G. S. Selwyn, *Phys. Plasmas* **1999**, *6*, 2284.
[188] M. Laroussi, *IEEE Trans. Plasma Sci.* **2002**, *30*, 1409.
[189] H. F. Windarto, T. Matsumoto, H. Akatsuka, M. Suzuki, *J. Nucl. Sci. Technol.* **2000**, *37*, 787.
[190] D. Purevdorj, N. Igura, M. Shimoda, O. Ariyada, I. Hayakawa, *Acta. Biotechnol.* **2001**, *21*, 333.
[191] F.-J. Trompter, W. J. Neff, O. Franken, M. Heise, M. Neiger, S. Liu, G. J. Pietsch, *IEEE Trans. Plasma Sci.* **2002**, *30*, 1416.
[192] N. S. Panikov, S. Paduraru, R. Crowe, P. J. Ricatto, C. Christodoulatos, K. Becker, *IEEE Trans. Plasma Sci.* **2002**, *30*, 1424.
[193] A. Soloshenko, V. V. Tsiolko, V. A. Khomich, Yu. V. Bazhenov, A. V. Ryabtsev, A. I. Scherdrin, I. L. Milkhno, *IEEE Trans. Plasma Sci.* **2002**, *30*, 1440.
[194] J.-C. Park, B. J. Park, D.-W. Han, D. H. Lee, I.-S. Lee, S. O. Hyun, M.-S. Chun, K.-H. Chung, M. Alhara, K. Takatori, *J. Microbiol. Biotechnol.* **2004**, *14*, 188.
[195] A. Sharma, A. Pruden, Z. Yu, G. J. Collins, *Envion. Sci. Technol.* **2005**, *39*, 339.
[196] A.-M. Pointu, A. Ricard, B. Dodet, E. Odic, J. Larbre, M. Ganciu, *J. Phys. D: Appl. Phys.* **2005**, *38*, 1905.
[197] R. E. J. Sladek, E. Stoffels, *J. Phys. D: Appl. Phys.* **2005**, *38*, 1716.
[198] H. Yu, S. Perni, J. J. Shi, D. Z. Wang, M. G. Kong, G. Shama, *J. Appl. Microbiol.* **2006**, *101*, 1323.
[199] R. Brandenburg, J. Ehlbeck, M. Stieber, T. V. Woedtke, J. Zeymer, O. Schluter, K. D. Weltmann, *Contrib. Plasma Phys.* **2007**, *47*, 72.
[200] Y.-T. Wu, J.-D. Liao, C.-C. Weng, M.-C. Wang, J.-E. Chang, C.-H. Chen, M. Zharnikov, *Contrib. Plasma Phys.* **2007**, *47*, 89.
[201] G. Fridman, A. D. Brooks, M. Balasubramanian, A. Fridman, A. Gutsol, V. N. Vasilets, H. Ayan, G. Friedman, *Plasma Process. Polym.* **2007**, *4*, 370.

[202] P. Brown, M. Preece, J. P. Brandel, T. Sato, L. McShane, I. Zerr, A. Fletcher, R. G. Will, M. Pocchiari, N. R. Cashman, J. H. d'Aignaux, L. Cervenakova, J. Fradkin, L. B. Schonberger, S. J. Collins, *Neurology* **2000**, *55*, 1075.
[203] A. Smith, M. Dickson, J. Aitken, J. Bagg, *J. Hosp. Infect.* **2002**, *51*, 233.
[204] X. T. Deng, J. Shi, H. L. Chen, M. G. Kong, *App. Phys. Lett.* **2007**, *90*, 013903.
[205] M. Moisan, J. Barbeau, M.-C. Crevier, J. Pelletier, N. Philip, B. Saoudi, *Pure Appl. Chem.* **2002**, *74*, 349.
[206] M. Yoshida, T. Tanaka, S. Watanabe, T. Takagi, M. Shinohara, S. Fujii, *J. Vac. Sci. Technol. A* **2003**, *21*, 1230.
[207] S. P. Sharma, B. A. Cruden, M. V. V. S. Rao, A. A. Bolshakov, *J. Appl. Phys.* **2004**, *95*, 3324.
[208] H. C. Baxter, G. A. Campbell, A. G. Whittaker, A. C. Jones, A. Aitken, A. H. Simpson, M. Casey, L. Bountiff, L. Gibbard, R. L. Baxter, *J. Gen. Virology* **2005**, *86*, 2393.
[209] O. Kylian, M. Hasiwa, F. Rossi, *IEEE Trans. Plasma Sci.* **2006**, *34*, 2606.
[210] H. Halfmann, N. Bibinov, J. Wunderlich, P. Awakowicz, *J. Phys. D: Appl. Phys.* **2007**, *40*, 4145.
[211] M. Vleugels, G. Shama, X. T. Deng, E. Greenacre, T. Brocklehurst, M. G. Kong, *IEEE Trans. Plasma Sci.* **2005**, *33*, 824.
[212] N. Abramzon, J. C. Joaquin, J. D. Bray, G. Brelles-Maria, *IEEE Trans. Plasma Sci.* **2006**, *34*, 1304.
[213] F. J. Critzer, K. Kelly-Wintenberg, S. L. South, D. A. Golden, *J. Food Protection* **2007**, *70*, 2290.
[214] S. Perni, D. W. Liu, G. Shama, M. G. Kong, *J. Food Prot.* **2008**, *71*, 302.
[215] J. Goree, B. Liu, D. Drake, E. Stoffels, *IEEE Trans. Plasma Sci.* **2006**, *34*, 1317.
[216] W. Stolz, M. Georgi, K. Ramrath, B. Peters, H.-U. Schmidt, R. Pompl, T. Shimizu, B. Steffes, W. Bunk, F. Jamitzky G. Morfill, *The First International Conference on Plasma Medicine*, Corpus Christi, Texas, USA, October 2007.
[217] G. Fridman, M. Peddinghaus, H. Ayan, A. Fridman, M. Balasubramanian, A. Gutsol, A. Brooks, G. Friedman, *Plasma Chem. Plasma Process.* **2006**, *26*, 425.
[218] L. F. Gaunt, C. B. Beggs, G. E. Georghiou, *IEEE Trans. Plasma Sci.* **2006**, *34*, 1257.
[219] S. Perni, G. Shama, J. L. Hobman, P. A. Lund, C. J. Kershaw, G. A. Hidalgo-Arroyo, C. W. Penn, X. T. Deng, J. L. Walsh, M. G. Kong, *Appl. Phys. Lett.* **2007**, *90*, 073902.
[220] D. L. Croteau, V. A. Bohr, *J. Biol. Chem.* **1997**, *272*, 25409.
[221] M. Laroussi, J. P. Richardson, F. C. Dobbs, *Appl. Phys. Lett.* **2002**, *81*, 772.
[222] X. T. Deng, J. J. Shi, M. G. Kong, *Appl. Phys. Lett.* **2005**, *87*, 153901.
[223] J. G. Birmingham, *IEEE Trans. Plasma Sci.* **2006**, *34*, 1270.
[224] X. T. Deng, J. J. Shi, M. G. Kong, *IEEE Trans. Plasma Science* **2006**, *34*, 1310.
[225] J. Raiser, M. Zenker, *J. Phys. D: Appl. Phys.* **2006**, *39*, 3520.
[226] K. R. Stalder, J. Woloszko, *Contrib. Plasma Phys.* **2007**, *47*, 64.
[227] J. G. Birmingham, *IEEE Trans. Plasma Sci.* **2006**, *34*, 1270.
[228] G. Fridman, A. Shereshevsky, M. M. Jost, A. D. Brooks, A. Fridman, A. Gutsol, V. Vasilets, G. Friedman, *Plasma Chem. Plasma Process.* **2007**, *27*, 163.
[229] E. Stoffels, I. E. Kieft, R. E. J. Sladek, *J. Phys. D: Appl. Phys.* **2003**, *23*, 2908.
[230] S. Yonson, S. Coulombe, V. Leveille, R. L. Leask, *J. Phys. D: Appl. Phys.* **2006**, *39*, 3508.

DOI: 10.1002/ppap.200700162